Thermalization in ultrarelativistic nuclear collisions. I. Parton kinetics and quark-gluon plasma formation

Klaus Geiger
School of Physics and Astronomy, University of Minnesota, Minneapolis, Minnesota 55455
(Received 10 March 1992)

A relativistic kinetic formulation of the time evolution of parton distributions during the early preequilibrium stage of nucleus-nucleus collisions at the BNL Relativistic Heavy Ion Collider (RHIC) and CERN Large Hadron Collider (LHC) is presented to study the microscopic dynamics and equilibration of the system. The nuclear collision is described as a sequence of multiple hard and soft parton-parton collisions and associated parton emission and absorption processes. Important aspects for the space-time evolution of the partonic system are the balance between emissive and absorptive processes, dilated formation of gluon radiation, and the effects of soft gluon interference. The time evolution of central $^{32}S+^{32}S$ and $^{197}Au+^{197}Au$ collisions at RHIC ($\sqrt{s} = 200A$ GeV) is studied in complete phase space and the approach to equilibrium is investigated. The results obtained imply the formation of hot quark-gluon plasmas in these collisions with estimated equilibration times, temperatures, and energy densities of $\tau_{eq} \simeq 1.2$ (1.8) fm/c, $T \simeq 290$ (325) MeV, and $\varepsilon \simeq 17$ (31) GeV/fm^3 for $^{32}S+^{32}S$ ($^{197}Au+^{197}Au$). The consequences of such rather high temperatures and energy densities should be clear quark-gluon plasma signatures, observable in the production of charm, strangeness, direct photons, and dileptons.

PACS number(s): 25.75.+r, 12.38.Bx, 12.38.Mh, 24.85.+p

I. INTRODUCTION

The possibility of producing dense plasmas of unconfined quarks and gluons in ultrarelativistic heavy-ion collisions may be realized in the near future in the planned collider experiments at the Relativistic Heavy Ion Collider (RHIC) at Brookhaven and the Large Hadron Collider (LHC) at CERN. In order to observe characteristic signals of quark-gluon plasma formation it is important to understand what happens at the very beginning, the "first few fm/c," of the nuclear collisions. It is usually assumed that the quanta which are produced in the central rapidity region quickly reach a state of local thermodynamic equilibrium. Such an assumption is the convenient basis of most theoretical studies addressing the properties of a quark-gluon plasma [1]. However, the validity of this assumption remains to be checked. In particular, one would like to know how the quanta evolve in phase space, if and under what circumstances they eventually thermalize, the time scale for this thermalization, the typical energy density and entropy soon after equilibration, etc. To study these questions systematically in a realistic model, a comprehensive description of the dissipative processes occurring during the *preequilibrium* phase of high-energy nuclear collisions has been developed in Ref. [2]. The model is based on the parton picture of hadronic interactions and describes the nuclear dynamics in terms of quark and gluon interactions within perturbative QCD, embedded in the framework of relativistic transport theory. The time evolution of the system is simulated by solving an appropriate transport equation in six-dimensional phase space with Monte Carlo methods.

In this and in a following paper [3] I report on the development of the work of Ref. [2] and present results of a quantitative analysis of the evolution of ultrarelativistic nuclear collisions towards equilibrium. The present paper is devoted mainly to the microscopic dynamics of partons and their approach to equilibrium. The second paper deals with the macroscopic thermodynamic properties of the system. The essential conclusion is that high-temperature quark-gluon plasmas can be formed in central $A + A$ collisions at RHIC ($E_{c.m.} = 200A$ GeV). In particular, for the two systems studied, $^{32}S + ^{32}S$ and $^{197}Au + ^{197}Au$, the estimates for the initial temperatures and energy densities of the plasmas are $T_0 \equiv T(\tau_{eq}) = 290$ MeV (325 MeV) and $\varepsilon \simeq 17$ (31) GeV/fm^3 for S+S (Au+Au).

In the parton cascade model presented here, the reaction mechanism is viewed as a succession of binary parton-parton collisions with associated radiative emission and absorption processes which are described as the evolution of multiple, internetted parton cascades. The approach incorporates the following important features.

(i) The parton distribution functions are evolved in full phase space and time; relativistic kinematics is used throughout.

(ii) The initial phase-space distribution of partons in the colliding nuclei is modeled on the basis of experimental knowledge of the flavor, momentum, and spatial parton substructure of nucleons.

(iii) The scale dependence of the initial parton distributions through the nuclear structure functions and their evolution according to renormalization-group improved perturbation theory is taken into account and computed dynamically in a self-consistent manner.

(iv) Several distinct interaction processes are included: lowest-order $2 \rightarrow 2$ scatterings, $1 \rightarrow 2$ decays, and $2 \rightarrow 1$ fusions supplemented by multiple radiative emission and absorption processes which correspond to the dominant contributions of higher-order QCD corrections to the Born amplitudes.

(v) A number of important effects that characterize the space-time evolution of a many parton system in nuclear collisions are accounted for: the individual time scale of each parton-parton collision and the formation time of parton radiation, the effective suppression of radiative emissions from virtual partons due to an enhanced absorption probability of others in regions of dense phase-space occupation, and the effects of soft gluon interference in low energetic gluon emissions.

Furthermore, a coalescence model for the final hadronization has been developed that recombines the partons into color neutral clusters when the perturbative evolution ceases to be valid and nonperturbative confinement mechanisms become essential. These clusters then decay into final observable hadrons. The hadronization scheme for the parton cascade model will be presented in a separate paper [4].

I believe that the model is suitable for the study of the equilibration process in ultrarelativistic nuclear collisions for the following reasons. The approach is almost exclusively based on the firmly established framework of perturbative QCD. The time evolution of the parton system in phase space according to the structure of interactions is rigorously calculated from a kinetic equation. The time variation of the parton densities, the number and type of interactions, etc., is determined by the dynamics itself. Attempts to model nonperturbative color exchange forces are avoided; rather, the perturbative evolution is cut off when it reaches its limits. The nonperturbative hadronization mechanism is considered within a completely separate model framework. Furthermore, these cutoff parameters which divide the perturbative from the nonperturbative domain are adjusted such that the perturbative parton cascade evolution reproduces the measured pp and $p\bar{p}$ cross sections over a wide range of energies, and, supplemented by the hadronization scheme, yields final particle distributions that agree with $p\bar{p}$ collider experiments at CERN and Fermilab Tevatron ($\sqrt{s}$=200–1800 GeV) [4].

The reliability of the model rests on the assumption that the dynamics is governed predominantly by independent parton-parton collisions plus associated parton emissions and absorption processes. If this assumption is correct, at least for the early evolution, then this model is probably the most appropriate description of ultrarelativistic nuclear collisions to date.

The study of the early stage of high-energy nuclear collisions has received rather scant attention. However, there are a number of works similar in spirit to the one presented here. A simple parton cascade model has been presented in Ref. [5]. Properties of parton thermalization have been addressed in Refs. [6–9] from a more phenomenological point of view. Recently, a two-stage equilibration scenario for gluons and quarks has been proposed within lowest-order perturbative QCD [10].

The organization of this paper is as follows. Sec. II is devoted to the description of the model. The relativistic kinetic framework is introduced and details of the newly included physics are explained. In Sec. III the results of simulations for central $^{32}S + ^{32}S$ and $^{197}Au + ^{197}Au$ collisions at RHIC energies are presented. Two distinct evolution scenarios for the collisions are compared and their characteristics are analyzed. Furthermore, predictions for thermalization times, temperatures, and energy densities are extracted. In Sec. IV some conclusions are drawn and possible observable consequences of the results are pointed out.

II. DESCRIPTION OF THE MODEL

In this section I establish a consistent kinetic framework based on the principles of relativistic transport theory. Furthermore, the essential concepts of the parton cascade model [2] are recalled and updated with emphasis on the newly included physics components.

A. The QCD transport equation

The basis of the model is a semiclassical, relativistic kinetic equation for the phase-space densities of quarks and gluons which can be solved by means of a Monte Carlo simulation. The partons are represented as classical point particles. The state of each parton is characterized by its type $a = q_f, \bar{q}_f, g$ (quarks, antiquarks of flavor f, and gluons), position $\mathbf{r}$, momentum $\mathbf{p}$, and its possible invariant virtuality M^2 corresponding to a spacelike ($M^2 < 0$) or timelike ($M^2 > 0$) virtual mass. The energy of a parton is therefore determined by $E_a^2 = \mathbf{p}^2 + m_a^2 + M^2 \geq 0$, where m_a is the flavor-dependent rest mass (with $m_u = 5.6$ MeV, $m_d = 9.9$ MeV, $m_s = 199$ MeV, $m_c = 1.35$ GeV, $m_b = 5$ GeV, and $m_g = 0$). The time-dependent phase-space density of partons of species a is represented by a Lorentz-invariant single-particle distribution function $F_a(p,r)d^3p\,d^3r/(2\pi)^3 2E$ depending on the four vectors $p = (E, \mathbf{p})$ and $r = (t, \mathbf{r})$. The transport equation has the manifestly invariant form

$$p^\mu \partial_\mu F_a(p,r) = \sum_{\text{processes } k} I_a^{(k)}(p,r) \tag{1}$$

with Lorentz-invariant collision integrals $I_a^{(k)}$. The left-hand side (LHS) of this Boltzmann-type equation describes the free propagation of partons, here generally taken to be on mass shell [11], whereas the collision term on the RHS represents a sum over all contributing interaction processes in which at least one parton of type a is involved.

Some remarks are opportune here (see also Sec. II F). The transport equation is, as it stands, a semiclassical formulation: it describes the evolution of a many-particle system in terms of single-particle distribution functions and classical particle trajectories. The quantum nature of the system is inherent exclusively in the collision term (as will be explained below). The latter models the space-time structure of parton interactions within the frame-

work of improved QCD perturbation theory via the relevant matrix elements and takes into account quantum statistical effects by using Fermi-Dirac and Bose-Einstein statistics for quarks and gluons, respectively. Note that long-range color forces are neglected and that no color mean field is included. It is important to realize that this transport equation is not derived from first principles of QCD. Rather it is a special case of Landau's kinetic equation which can be deduced from the general many-body Schrödinger equation within the statistical approach of particle transport theory, or alternatively from classical many-body theory.

In order to solve the transport equation (1) for the time evolution of the parton distributions in phase space, one needs to specify (i) the initial parton distributions in the incoming nuclei and (ii) the form of the collision term, that is the parton interaction processes to be considered.

B. The initial state

Choosing the center-of-mass (c.m.) frame of the colliding nuclei as the reference frame, with the collision axis in the z direction, the nucleons carry equal fractions of the c.m. momenta $\pm\mathcal{P}_{\rm c.m.}$ of the nuclei A and B, $\mathbf{P} = (0, 0, \pm\mathcal{P}_{\rm c.m.}/N_{A,B})$, where $+$ $(-)$ refers to the nucleons of nucleus A (B) and N_A (N_B) is the number of nucleons in A (B).

The initial phase-space distribution F_a^0 of the partons in the incoming nuclei A and B generally depends on the total beam energy, $s = E_{\rm c.m.}^2$, as well as on the parton momenta and positions at time $t = t_0$, the moment the nuclei collide. For each of the two nuclei it is chosen to be a superposition of parton distributions in the individual nucleons

$$F_a^0(s; E, \mathbf{p}, \mathbf{r}, t = t_0) = \sum_{i=1}^{N_{\rm nuc}} P_a^{N_i}(E, \mathbf{p}, \mathbf{P}) \cdot R_a^{N_i}(\mathbf{p}, \mathbf{r}, \mathbf{R})\Big|_{t=t_0} . \quad (2)$$

Here $P_a^{N_i}$ and $R_a^{N_i}$ give the initial momentum and spatial distribution, respectively, for partons of type a in each individual nucleon N_i inside the nuclei and the sum runs over all $N_{\rm nuc} = N_A + N_B$ nucleons in nucleus A and nucleus B. The vectors $\mathbf{p}, \mathbf{P}$ and $\mathbf{r}, \mathbf{R}$ denote the momenta and coordinates of partons, respectively, nucleons. The parton energies $E \equiv E_a(M^2) = \sqrt{\mathbf{p}^2 + m_a^2 + M^2}$ take into account their initial spacelike virtualities $M^2 < 0$ as an independent variable.

For each nucleon the number of partons, the distribution of the flavors, their momenta, and associated initial spacelike virtualities are obtained from

$$P_a^{N_i}(E, \mathbf{p}, \mathbf{P}) = \frac{x}{\tilde{x}} f_a^{N_i}(x, Q_0^2) g(\mathbf{p}_\perp) \quad (3)$$

with the momentum and energy fractions ($P = |\mathbf{P}|$)

$$x = \frac{p_z}{P}, \quad (4)$$

$$\tilde{x} = \frac{E}{P} = \sqrt{x^2 + \frac{p_\perp^2 + m_a^2 + M^2}{P^2}} \quad (5)$$

and the normalizations

$$\sum_a \int x f_a^{N_i}(x, Q_0^2) dx = \int g(\mathbf{p}_\perp) d^2 p_\perp = 1, \quad (6)$$

$$\sum_a \int P_a^{N_i}(E, \mathbf{p}, \mathbf{P}) \frac{d^3 p}{(2\pi)^3} = n^{N_i}(\mathbf{P}) . \quad (7)$$

The functions $f_a^{N_i}(x, Q_0^2)$ are the scale-dependent measured nucleon structure functions with x being the fraction of the parent nucleons longitudinal momentum P carried by the parton. The labels N_i and a characterize the type of nucleon and parton, respectively. The set of structure functions employed in this work is the higher-order parametrization of Glück, Reya, and Vogt [12]. The transverse momentum distribution $g(p_\perp)$ is specified below. The factor $x/\tilde{x}$ in Eq. (3) is included to form the invariant momentum integral $\int d^3p/(2\pi)^3 2E$ out of the distribution $P_a^{N_i}$. In (7) n^{N_i} refers to the number of partons in a given nucleon.

The *resolution scale* Q_0^2 at which the structure functions $f_a^{N_i}(x, Q_0^2)$ must be evaluated has the physical meaning of how detailed the partons of one nucleus "see" the parton structure of the other nucleus. In practice, Q_0^2 is computed on a statistical basis of simulating many nuclear collision events. Before the first collision Q_0 is chosen to be a lower limit of 1 GeV. For the following events, Q_0 is set equal to the average momentum transfer of those parton-parton collisions that involve at least one primary parton. This average value is estimated from accumulated statistics up to the previous collision event. This procedure converges rather fast, yielding a Q_0 of the order of a few GeV, since most of the parton collisions involve a relatively small momentum transfer. The magnitude of Q_0 depends only weakly on the beam energy and the mass of the beam nuclei. In addition, primary parton collisions with a momentum transfer $\gg Q_0^2$, which correspond to rare fluctuations, are taken into account individually by the Q^2 evolution of the nucleon structure functions through spacelike radiation processes (see Sec. II C below).

The primordial transverse momenta of partons are distributed according to the function $g(\mathbf{p}_\perp)$, chosen to be a Gaussian $\sim \exp(-|\mathbf{p}_\perp|^2/p_0^2)$, independent of the type of parton or nucleon. It takes into account the uncertainty of momentum due to the partons' confinement within the nucleon. The width p_0 is adjusted so that the invariant mass of the parton distribution of each nucleon equals the nucleon mass: $(\sum_i E^i)^2 - (\sum_i p_x^i)^2 - (\sum_i p_y^i)^2 - (\sum_i p_z^i)^2 = M_{\rm nuc}^2$. Here the sums run over all partons in a nucleon, their number n being determined by the conditions (6) and (7). The resulting value $p_0 \approx 0.42$ GeV/c, corresponding to $\langle p_\perp \rangle \approx 0.38$ GeV/c, agrees well with values inferred from experimental data [13–15].

The initial spatial distribution of partons appearing in Eq. (2), $R_a^{N_i}$, depends on the magnitude of their momenta, the positions of their parent nucleons and on the

spatial substructure of the latter. It is represented as

$$R_a^{N_i}(\mathbf{p},\mathbf{r},\mathbf{R}) = [\,h_a^{N_i}(\mathbf{r})H_{N_i}(\mathbf{R})\,]_{\text{boosted}}, \tag{8}$$

where $i = 1,\ldots,N_{\text{nuc}}$ and the p dependence is assumed to result purely from boosting the distributions to the nuclear c.m. frame (see below). It is obtained as follows: The incoming nuclei are given their initial c.m. positions corresponding to a chosen impact parameter. Then, in the rest frame of each nucleus, the individual nucleons are assigned positions around the centers of their parent nuclei according to a Fermi distribution for nuclei with mass number $A \geq 12$ and a Gauss distribution for nuclei $A < 12$:

$$H_{N_i}(\mathbf{R}) = \begin{cases} \frac{1}{4\pi}\{1+\exp[(R-c)/a]\}^{-1} & (A \geq 12), \\ \frac{1}{4\pi}\frac{2}{\sqrt{\pi}b}\exp[-R^2/b^2] & (A < 12). \end{cases} \tag{9}$$

The parameters are $c = r_0 A^{1/3}$, $r_0 = 1.14$ fm, $a = 0.545$ fm and $b = \sqrt{2/3}R_{\text{ms}}$, where R_{ms} is the mean-square radius of the nucleus.

The partons are distributed around the centers of the nucleons, still in the rest frame of the actual nucleus, with an exponential distribution

$$h_a^{N_i}(\mathbf{r}) = \frac{1}{4\pi}\frac{\nu^3}{8\pi}\exp[-\nu r], \tag{10}$$

where $\nu = 0.84$ GeV/c corresponds to the measured elastic form factor of the nucleon with a mean-square radius of $R_{\text{nuc}} \equiv \sqrt{12/\nu} = 0.81$ fm.

Finally, as indicated by the subscript "boosted" in Eq. (8), the positions of the nucleons and their valence quarks are boosted into the c.m. frame of the colliding nuclei. The sea quarks and gluons are smeared out in the longitudinal direction by an amount $\Delta z \approx \hbar/p_z < 2R_{\text{nuc}}$ around the valence quarks. This procedure yields the *distributed Lorentz contraction* which is an important feature of the partons when boosting a nucleus to high rapidities [6,16,17]. As a consequence, the parton positions are correlated in longitudinal direction with their momenta, as required by the uncertainty principle.

C. The space-time structure of parton kinetics

The evolution of the parton distributions due to interactions among the quanta has been extended considerably since the previous version of the model [2]. In particular, (i) hard and semihard parton-parton collisions, described within perturbative QCD, are supplemented by "soft" interactions below a critical momentum transfer, (ii) newly included perturbative recombination processes, described as parton fusions, are treated on the same footing as parton-parton collisions, (iii) the radiative emission of gluons is now balanced by the reverse processes of gluon absorption, (iv) the formation time of the radiation and its specific space-time evolution according to the Landau-Pomeranchuk effect [18] is incorporated, and (v) the suppression of radiative emissions resulting from destructive interference of soft emitted gluons is taken into account.

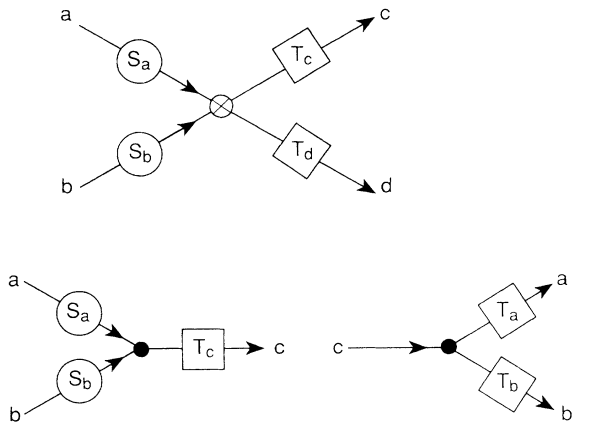

FIG. 1. Schematical illustration of the three general types of parton interactions that are considered to contribute to the collision term (11): $2 \to 2$ collisions [Eq. (12)], $2 \to 1$ fusions, and $1 \to 2$ decays [Eq. (13)]. Each of the partons coming into (emerging from) a vertex is dressed by an S (T) form factor taking into account higher-order perturbative QCD corrections. The S form factors include radiative corrections from primary spacelike partons having their first collisions, whereas the T form factors account for multiple emissions and absorptions by timelike secondary partons. Note that there is no S form factor for the $1 \to 2$ branchings, because these processes occur only for timelike excited partons originating from previous collisions or decays.

Recall that the collision term on the RHS of the transport equation (1) generally includes all possible $n \to n'$ interaction processes. Each term of the sum over contributing processes is a phase-space integral involving the corresponding squared matrix elements $|M_{n\to n'}|^2$. In the parton cascade approach presented here, a subset of $n \to n'$ processes is considered which consists of $2 \to 2$ collisions, $2 \to 1$ fusions, and $1 \to 2$ decays in lowest-order perturbation theory. These are supplemented by higher-order corrections which are associated with multiple emissions and absorptions of partons. Correspondingly, the collision term is represented as a sum over all possible lowest-order $2 \to 2$, $2 \to 1$, and $1 \to 2$ parton interactions, in which each of the partons coming in and going out of the vertices is "dressed" by a specific form factor that includes the QCD radiative corrections in the leading-logarithmic approximation [19,20]. This concept is schematically illustrated in Fig. 1.

The collision term in Eq. (1) changes the phase-space distribution $F_a(p,r)$ of parton species a at the space-time point $r = (t,\mathbf{r})$ due to interactions in which a parton a may be gained or lost in a phase-space element $d^3p/(2\pi)^3 2E$. It is represented as

$$\sum_{\text{processes } k} I_a^{(k)}(p_1,r) = \sum_{b,c,d} J_{abcd}(p_1,r) + \sum_{b,c} K_{abc}(p_1,r). \tag{11}$$

The two distinct types of interaction integrals J and K are given by the difference of gain and loss terms (with respect to partons of species a) for $2 \to 2$ and for $2 \to 1$, $1 \to 2$ processes, respectively. Specifically,

$$J_{abcd}(p_1,r) = j^{\rm gain}_{cd\to ab}(p_1,r) - j^{\rm loss}_{ab\to cd}(p_1,r)$$
$$= -\frac{1}{2}\left(\frac{1}{1+\delta_{ab}}\right)\left(\frac{1}{1+\delta_{cd}}\right)\int\frac{d^3p_2}{(2\pi)^3 2E_2}\int\frac{d^3p_3}{(2\pi)^3 2E_3}\int\frac{d^3p_4}{(2\pi)^3 2E_4}$$
$$\times\{F_a(1)F_b(2)[1\pm F_c(3)][1\pm F_d(4)] - F_c(3)F_d(4)[1\pm F_a(1)][1\pm F_b(2)]\}$$
$$\times(2\pi)^4\delta^4(p_1+p_2-p_3-p_4)\sum|M_{ab\to cd}|^2_{\rm eff}, \tag{12}$$

and

$$K_{abc}(p_1,r) = k^{\rm gain}_{c\to ab}(p_1,r) - k^{\rm loss}_{ab\to c}(p_1,r)$$
$$= -\frac{1}{2}\left(\frac{1}{1+\delta_{ab}}\right)\int\frac{d^3p_2}{(2\pi)^3 2E_2}\int\frac{d^3p_3}{(2\pi)^3 2E_3}(2\pi)^4\delta^4(p_1+p_2-p_3)$$
$$\times\left\{F_a(1)F_b(2)[1\pm F_c(3)]\sum|M_{ab\to c}|^2_{\rm eff} - F_c(3)[1\pm F_a(1)][1\pm F_b(2)]\sum|M_{c\to ab}|^2_{\rm eff}\right\}. \tag{13}$$

In expressions (12) and (13) I introduced the notation $F_\alpha(i)\equiv F_\alpha(p_i,r)$ for the distribution functions of parton species $\alpha = a,b,c,d$ and corresponding four-momenta $p_i = p_1,p_2,p_3,p_4$ at space-time point $r=(t,\mathbf{r})$. The squared matrix elements, characteristic for the types of interactions, are weighted by a distribution function F_α for each of the particles coming into the interaction vertex and a factor $[1\pm F_\alpha]$ for each of the outgoing ones. The minus sign refers to quarks and antiquarks with $[1-F_q]$ indicating Pauli blocking, and the plus sign is for gluons so that $[1+F_g]$ results in a Bose enhancement. The factors $1/(1+\delta_{ab})$ and $1/(1+\delta_{cd})$ account for the cases where the two incoming and/or outgoing partons are identical. Finally, the factors $1/2$ in front of the RHS of Eqs. (12) and (13) result from the normalization $1/2E_1$.

The *effective squared matrix elements* $\sum|M|^2_{\rm eff}$ are expressed in terms of the lowest-order matrix elements $\sum|M^{(0)}|^2$ summed over spin and color, and are multiplied by S (spacelike) and T (timelike) form factors for the partons coming in, respectively, going out of, the vertex (see Fig. 1). That is,

$$\sum|M_{ab\to cd}|^2_{\rm eff} = S_a(p_a;Q^2,Q_0^2)\;S_b(p_b;Q^2,Q_0^2)\sum|M^{(0)}_{ab\to cd}|^2(Q^2)T_c(Q^2,\mu_0^2)\;T_d(Q^2,\mu_0^2), \tag{14}$$
$$\sum|M_{ab\to c}|^2_{\rm eff} = S_a(p_a;p_c^2,Q_0^2)\;S_b(p_b;p_c^2,Q_0^2)\sum|M^{(0)}_{ab\to c}|^2(p_c^2)\;T_c(p_c^2,\mu_0^2), \tag{15}$$
$$\sum|M_{c\to ab}|^2_{\rm eff} = \sum|M^{(0)}_{c\to ab}|^2(p_c^2)\;T_a(p_c^2,\mu_0^2)\;T_b(p_c^2,\mu_0^2). \tag{16}$$

The lowest-order invariant squared matrix elements $\sum|M^{(0)}|^2$ are well known for the elementary processes specified below and the form factors are introduced in Sec. II E. The distribution functions $F_\alpha(p,r)$ in Eqs. (12) and (13) on the other hand are not available in analytic form since they are determined by the dynamics itself. During the cascade evolution, they can be estimated by dividing phase space into cells and counting the number of partons $n_\alpha(k)$ in each cell k for each species α individually at a given point of time [3]:

$$F_\alpha(p,r)\;\to\;\bar F_\alpha(k) = \frac{n_\alpha(k)}{\gamma_\alpha\int_k d^3p\,d^3r/(2\pi)^3}. \tag{17}$$

Here γ_α is the product of degeneracy factors for spin and color associated with parton species α: $\gamma_g = 2\times 8$ and $\gamma_q = \gamma_{\bar q} = 2\times 3$. The quantum statistical effects of Pauli blocking for quarks and Bose enhancement for gluons are accounted for in the simulation by multiplying the squared matrix elements for each process by the estimated distribution factors $[1-\bar F_q(k)]$ and $[1+\bar F_g(k)]$ for quarks and gluons, respectively, with k referring to the phase-space cell at $\mathbf{p}$ and $\mathbf{r}$.

To elucidate the physical significance of the effective matrix elements (14)–(16), a number of remarks are helpful:

(i) In (14), Q^2 specifies the invariant scale at which the interaction occurs. It generally depends on the four-momenta of the scattering partons and is not unambiguous in lowest-order perturbation theory. It is chosen to be the transverse momentum of the scattered partons in their c.m. frame, $Q^2 = p_\perp^2$, except for $q\bar q$ annihilation where $Q^2 = (E^2_{q\bar q})_{\rm c.m.}$. The value of Q^2 determines the strength of the QCD coupling $\alpha_s(Q^2)$ associated with the vertex.

(ii) Q_0^2 is the (small) resolution scale at which the colliding nuclei initially were resolved into their parton substructure [cf. after Eq. (7)] and μ_0^2 is an invariant-mass cutoff below which parton emission is considered to be unresolvable. The values of Q_0^2 and μ_0^2 define the initial and final point, respectively, between which the evolution of parton cascades is followed perturbatively. The

nonperturbative dynamics outside this regime must be absorbed in the initial parton distributions (2) depending on Q_0^2 (via the nuclear structure functions) and in the final hadronization of partons which takes effect below μ_0^2.

(iii) The representations (14)–(16) may be pictured as elastic processes with the incoming and outgoing partons being off mass shell or "dressed," corresponding to higher-order inelastic contributions. Setting the form factors S and T equal to unity therefore corresponds to treating the external particles as bare quanta on mass shell.

(iv) The phenomenological difference between the S and T form factors is important to realize. The S form factors are of relevance only for primary spacelike partons that evolve directly from the initial nuclear parton clouds and encounter their first interaction. For all other (secondary) partons, those that have either emerged from a scattering or been produced in a decay process, S is equal to unity. Furthermore, one might get the impression that the T form factors only "dress" those partons that emerge from an interaction vertex. However, these "dressed" partons can subsequently interact again, so that the T form factors are implicitly present also in those interactions where timelike partons are incoming to the vertex. To avoid double counting, therefore only the partons receding from a vertex are "dressed" by a T form factor in Eqs. (14)–(16).

At this point I would like to comment briefly on the properties of *detailed balance* of the various interaction processes taken into account in the collision integrals (12) and (13) and the implications for equilibration of the parton system. When the collision term (11) becomes zero, the parton distribution functions provide a stationary solution to the transport equation (1). During the evolution of nuclear collisions there are basically two cases when the collision term can vanish locally: (i) in the central region, when the system of partons reaches a state of detailed balance with respect to the contributing $2 \to 2$, $2 \to 1$, $1 \to 2$ processes, implying equilibration, and (ii) when the partons in the beam fronts are fast receding from the collision region and are approaching free streaming.

In general the interaction processes contributing to the collision term (11) processes fall into two categories; namely, processes that do not change the number of quarks and antiquarks, and those that alter the quark flavor composition. For the $2 \to 2$ processes these are

$$a + b \to a + b \,, \tag{18}$$

$$a + \bar{a} \to c + \bar{c} \tag{19}$$

($a, b = q, \bar{q}, g$ and $c = q$), where (18) corresponds to elastic scattering and the annihilation process (19) is a "chemical reaction" that changes the number of quarks. The inelastic processes $2 \to 1$ and $1 \to 2$, which produce or annihilate one gluon, are

$$a \leftrightarrow a + g \,, \tag{20}$$

$$g \leftrightarrow c + \bar{c} \,. \tag{21}$$

Here (20) is a gluon emission ($\to$) or an absorption ($\leftarrow$) process with parton a appearing in both initial and final state. The process (21) is a "chemical reaction" that increases (reduces) the number of quark-antiquark pairs.

Semiclassical kinetic theory [21] states that when the system is in local equilibrium with respect to the elastic binary collisions (18) and the gluon emission and absorption processes (20), then the distribution functions in phase space for the various species a, $F_a(p,r)$, take the form

$$F_a^{\pm}(p,r) = \frac{1}{\exp[\beta_\nu(p^\nu - \lambda_a^\nu)] \pm 1} \,. \tag{22}$$

Here p_ν is the four-momentum of the particle and the upper sign refers to fermions (quarks) and the lower sign to bosons (gluons). $\lambda_\nu(r)$ and $\beta_\nu(r)$ are four vectors constructed from the local flow velocity $u_\nu(r)$, the local chemical potentials $\mu_a(r)$ (one for each quark species), and the inverse local temperature $\beta(r) = 1/T(r)$:

$$\lambda_a^\nu(r) = \mu_a(r) u^\nu(r) \,, \tag{23}$$

$$\beta^\nu(r) = \beta(r) u^\nu(r) \,. \tag{24}$$

The nonvanishing chemical potentials μ_a for flavor a are the parameters which measure the number of quarks minus antiquarks. In the baryon-free central rapidity region they give the deviation from complete chemical equilibrium. In addition, equilibrium with respect to the "chemical reactions" (19) and (21) requires that the sum of the chemical potentials of the particles on the LHS equals the sum on the RHS for each process [22]. This can easily be verified by inserting the distribution functions (22) into the collision integrals and using the identity $1 \mp F^{\pm} = \exp[\beta_\nu(p^\nu - \lambda_a^\nu)] F^{\pm}$. For the processes (19), the equilibrium conditions are

$$\mu_a + \mu_{\bar{a}} = \mu_c + \mu_{\bar{c}} \,, \tag{25}$$

$$\mu_a + \mu_{\bar{a}} = 2\mu_g \,, \tag{26}$$

and, for the processes (21),

$$\mu_a + \mu_{\bar{a}} = \mu_g \,. \tag{27}$$

Consequently, from (26) and (27), one sees that the gluon chemical potential must vanish and therefore $\mu_a = -\mu_{\bar{a}}$. On the other hand, in a baryon-free plasma particle-antiparticle symmetry imposes $\mu_a = \mu_{\bar{a}}$, so that the conditions (25)–(27) imply

$$\mu_g = 0 \,, \tag{28}$$

$$\mu_a = \mu_{\bar{a}} = 0 \,, \tag{29}$$

and the latter equality must hold for each quark flavor individually.

Thus, in the approximately baryon-free central region, a complete thermal and chemical equilibrium is established, if the system is characterized by detailed balance

with respect to the processes (18)–(21), that is by vanishing chemical potentials for all quark flavors.

As far as the baryon-rich nuclear fragmentation region is concerned, the collision term becomes very small at times when the fast partons in the beam fronts approach free streaming and move collinearly away from the central region. In this case the parton densities become dilute and the probability of two partons a and b to collide, $dP_{ab} \propto \sqrt{(p_a \cdot p_b)^2 - m_a^2 m_b^2}\, d\hat{\sigma}_{ab}$, tends to zero.

D. Lowest-order contribution to the collision term

The lowest-order contribution to the collision integrals (11) is equivalent to setting the form factors in the effective squared matrix elements (14)–(16) equal to unity, $\sum |M|^2_{\rm eff} \to \sum |M^{(0)}|^2$. This corresponds to retaining only the lowest-order Born terms for $2 \to 2$ collisions, $2 \to 1$ fusions, and $1 \to 2$ decays of partons.

1. $2 \to 2$ collisions

Two distinct classes of processes $a+b \to c+d$ are considered: (i) hard and semihard parton scatterings in the framework of perturbative QCD; (ii) soft parton interactions modeled as low momentum transfer, two-gluon-exchange processes. The motivation for this differentiation of parton-parton collisions is to smoothen the singular behavior of the collision integrals (12) which results from the divergence of the squared matrix elements for small momentum transfers (except for $q\bar{q}$ annihilation). Clearly, this is due to the long-range nature of the color forces, or more precisely, to the fact that many-particle correlations, which provide the Debye shielding, are not included in the transport equation. The heuristic procedure for incorporating collective effects of a many-parton system into binary collision theory is to introduce a cutoff at the Debye screening length. Long-range interactions may be incorporated in terms of an expansion with respect to small momentum transfers in collisions [23,24].

In the present model, an invariant cutoff scale $Q^2_{\rm cut} \equiv p^2_{\perp\rm cut}$ is introduced such that collisions with $p_\perp \geq p_{\perp\rm cut}$ are treated as (semi)hard scatterings within QCD perturbation theory, whereas for $p_\perp < p_{\perp\rm cut}$ a soft interaction is assumed to occur. From an analysis of pp and $p\bar{p}$ cross sections [25] it was concluded that this cutoff depends on the beam energy. It was shown that the parametrization

$$p_{\perp\rm cut} = a \left(\frac{s_{\rm beam}}{s_0} \right)^b \tag{30}$$

with $a = 0.35$ GeV/c, $b = 0.14$, and $s_0 = 1$ GeV^2 reproduces the pp and $p\bar{p}$ cross section for a wide range of energies. For the case of nuclear collisions the cutoff $p_{\perp\rm cut}$ might be replaced by the Debye screening mass in the gluon propagator, $p^2_{\perp\rm cut} \simeq m_g^2 = g_s^2 T^2$ [26], and similarly, $p^2_{\perp\rm cut} \simeq m_q^2 = g_s^2 T^2/6$ [27] in the quark propagator, where g_s is the strong coupling and T the local temperature. However, these features are not included yet and remain to be studied in the future. Instead, for $A+A$ collisions the $p_{\perp\rm cut}$ value is chosen according to the form (30) with the replacement $\sqrt{s_{\rm beam}} \to \sqrt{s_{\rm beam}}/A$.

The following $2 \to 2$ interaction processes are included:

$$\begin{aligned} &gg \to gg, \quad gg \to q\bar{q}, \quad qg \to qg, \quad \bar{q}g \to \bar{q}g, \\ &qq \to qq, \quad \bar{q}\bar{q} \to \bar{q}\bar{q}, \quad q\bar{q} \to q'\bar{q}', \quad q\bar{q} \to gg. \end{aligned} \tag{31}$$

For the perturbative (semi)hard collisions above $p_{\perp\rm cut}$, the momentum transfer $\hat{t}$ is determined by the corresponding differential cross sections

$$\frac{d\hat{\sigma}^{\rm hard}_{ab\to cd}}{d\hat{t}} = \frac{1}{16\pi \hat{s}^2} \sum |\bar{M}^{(0)}_{ab\to cd}|^2(Q^2, \hat{s}, \hat{t}, \hat{u}), \tag{32}$$

where $\hat{s} = (p_a + p_b)^2$, $\hat{t} = (p_a - p_c)^2$, $\hat{u} = (p_a - p_d)^2$, $Q^2 = p_\perp^2 \simeq \hat{t}\hat{u}/\hat{s}$, and $\sum |\bar{M}^{(0)}|^2$ is the spin- and color-averaged squared matrix element in lowest-order perturbation theory. For the processes (31) the cross sections are published in the literature [28].

In the case of a soft interaction between two partons, below $p_{\perp\rm cut}$, it is assumed that a very low energy double-gluon exchange occurs. This provides a natural continuation to the harder collisions above $p_{\perp\rm cut}$ where the dominant one-gluon-exchange processes $gg \to gg$, $gq \to gq$, and $qq \to qq$ have the same overall color structure [29]. The momentum transfer $\hat{t}$ between two soft interacting partons is chosen according to the simple phenomenological distribution

$$\frac{d\hat{\sigma}^{\rm soft}_{ab\to cd}}{d\hat{t}} = f(E^2_{\rm c.m.}, \hat{t}_{\perp\rm cut}) \exp\left[\frac{\hat{t} - \hat{t}_{\rm cut}}{\hat{t}_0} \right], \tag{33}$$

where $E_{\rm c.m.} = \sqrt{s_{\rm beam}}/A$, $\hat{t}_0 = 1$ GeV^2 and

$$\hat{t}_{\rm cut} \simeq -\frac{\hat{s}}{2} \left(1 - \sqrt{1 - \frac{4p^2_{\perp\rm cut}}{\hat{s}}} \right). \tag{34}$$

The factor

$$f(E^2_{\rm c.m.}, \hat{t}_{\perp\rm cut}) = \frac{\hat{\sigma}^{\rm inel}(E^2_{\rm c.m.}) - \hat{\sigma}^{\rm hard}(E^2_{\rm c.m.})}{\exp[-\hat{t}_{\perp\rm cut}/\hat{t}_0] - 1} \tag{35}$$

is determined by the requirement that the sum $\hat{\sigma}^{\rm inel} = \hat{\sigma}^{\rm soft} + \hat{\sigma}^{\rm hard}$ per nucleon corresponds to the measured inelastic pp and $p\bar{p}$ cross sections for given beam energy $\sqrt{s_{\rm beam}}/A$. Thus, the soft contribution adds to the total inelastic cross section what is left out by (semi)hard parton collisions.

2. $2 \to 1$ and $1 \to 2$ processes

In lowest-order perturbation theory the possible $2 \to 1$ fusion processes among partons are

$$gg \to g^*, \quad q\bar{q} \to g^*, \quad qg \to q^*, \tag{36}$$

where the asterisk indicates that the produced parton is off mass shell. Correspondingly, the reverse $1 \to 2$ decay processes are

$$g^* \to gg, \quad g^* \to q\bar{q}, \quad q^* \to qg. \tag{37}$$

The fusion processes (36) have the same initial states as the $2 \to 2$ collisions (31) and therefore compete with

the latter. The relative probability of whether two partons a and b ($ab = gg; q\bar{q}; qg$) scatter from each other, $ab \to e^* \to cd$, or fusion, $ab \to e^*$, is determined by treating the virtual parton e^* as a resonance with a proper lifetime associated with its virtuality and the possible decay channels $e^* \to cd$. The lifetime of a parton e^* with virtuality $p_{e^*}^2 = q^2$ is related to the inverse of its decay width in the c.m. frame:

$$\Gamma_{e^*}(Q) = \frac{1}{2Q} \sum_{c,d} \int \frac{d^3p_1}{(2\pi)^3 2E_1} \int \frac{d^3p_2}{(2\pi)^3 2E_2} (2\pi)^4 \delta^4(q - p_1 - p_2)[1 \pm F_a(1)][1 \pm F_b(2)] \sum |\bar{M}_{e^* \to cd}|^2 , \tag{38}$$

where $q = (Q, \mathbf{0})$. $\sum |\bar{M}|^2$ is the appropriate spin- and color-averaged matrix-element squared weighted with the distribution factors $[1 \pm F]$ for the decay products. In order to obtain an analytical expression for the width, the factors $[1 \pm F]$ are approximated by unity, i.e., $F \ll 1$ and the partons c, d are assumed to be on mass shell. Then the decay rate (38) is readily evaluated in lowest order. In the laboratory frame the Lorentz-dilated lifetime $\tau_{e^*} = \gamma/\Gamma_{e^*}$ of a parton e^* is

$$\begin{aligned} \tau_{q^*}(Q) &\equiv \left(\frac{E_{q^*}}{Q}\right) [\Gamma_{q^* \to qg}(Q)]^{-1} \\ &= \frac{3E_{q^*}}{2\alpha_s Q^2} \left[\left(1 - \frac{2m_q}{Q} + \frac{m_q^2}{Q^2}\right)\left(1 - \frac{2m_q^2}{Q^2} + \frac{m_q^4}{Q^4}\right)^{1/2}\right]^{-1} , \\ \tau_{g^*}(Q) &\equiv \left(\frac{E_{g^*}}{Q}\right) [\Gamma_{g^* \to gg}(Q) + \Gamma_{g^* \to q\bar{q}}(Q)]^{-1} \\ &= \frac{E_{g^*}}{2\alpha_s Q^2} \left[1 + \frac{1}{8} \sum_q \left(1 + \frac{2m_q^2}{Q^2}\right)\left(1 - \frac{4m_q^2}{Q^2}\right)^{1/2}\right]^{-1} , \end{aligned} \tag{39}$$

where the sum in the expression for τ_{g^*} runs over the quark flavors with $m_q^2 \leq Q^2/4$ and

$$\alpha_s \equiv \alpha_s(Q^2) = \frac{12\pi}{(33 - 2n_f)\ln(Q^2/\Lambda^2)} \tag{40}$$

is the running QCD coupling strength. The probability that a virtual parton e^* decays within a given time interval Δt in the laboratory frame is then determined by

$$\Pi_{e^*}(Q, \Delta t) = 1 - \exp[-\Delta t/\tau_{e^*}(Q)]. \tag{41}$$

It is important to realize that the use of Eq. (41) relies on the intuitive, classical point of view which pictures virtual partons as unstable particles that will live for a time τ, determined by the degree to which they are off mass shell, and then decay. Clearly Eqs. (39)–(41) serve only as a rough prescription for estimating the effect of the uncertainty principle. A more rigorous, quantum mechanical treatment would be desirable, but remains to be developed.

In practice the combination of $2 \to 2$, $2 \to 1$, and $1 \to 2$ processes is simulated as follows: Since the time evolution of the parton system is described in small discrete time steps Δt ($= 10^{-2}$ fm/c), the time scale of an interaction process is compared with Δt to decide whether the interaction occurs within this time interval. A virtual parton e^* produced via $a + b \to e^*$ has a short lifetime τ_{e^*} if its invariant mass Q^2 is large and it is likely to decay within Δt. Therefore, the $2 \to 2$ process $a + b \to e^* \to c + d$ preferably occurs. On the other hand, if Q^2 is small, corresponding to a long τ_{e^*}, parton e^* will probably not decay within Δt and the fusion process $a + b \to e^*$ rather happens. In this case, e^* propagates as a quasistable particle until in the following time step it has an increased decay probability $\Pi_{e^*}(Q, 2\Delta t)$. This may then result in the $1 \to 2$ decay $e^* \to c + d$. Alternatively, e^* might collide with another parton before its decay or may propagate freely until the following time step, and so on.

E. Higher-order corrections to the collision term

The contributions of $2 \to 2$ collisions, $2 \to 1$ fusions, and $1 \to 2$ decays to the collision term (11) correspond to the Born terms of lowest-order perturbation theory. However, as is well known, higher-order terms are enhanced by large logarithms arising from the singularities of radiative corrections. These can be described by multiple parton branching processes, that is, in terms of chains of successive elementary $1 \to 2$ parton branchings $q \to qg$, $g \to gg$, $g \to q\bar{q}$ [2,19,20,30]. In the kinetic formulation of Sec. II C these radiative processes are represented by the S and T form factors in the effective matrix elements (14)–(16) (see Fig. 1).

The QCD branching processes occur in two different

contexts: spacelike and timelike branchings. Spacelike branchings arise exclusively from the primary partons. If such a parton scatters for the first time at some scale $Q^2 > Q_0^2$, its initial small spacelike virtuality $|q_0|^2 \approx Q_0^2$ increases as a result from successive parton branchings up to $|q|^2 \approx Q^2$. Timelike branchings, on the other hand, may be regarded as sequences of branchings that are initiated either by one or both of a pair of scattered partons, or by a single timelike virtual parton. The parton decreases its timelike virtuality M^2 by successive branchings until either the chain is interrupted by a collision with another parton, or the virtualities of the radiated partons fall below some cutoff μ_0^2 beyond which nonperturbative mechanisms are dominant.

In high-energy collisions of heavy nuclei this picture of independent cascades of successive parton branchings will be modified by a number of important effects.

(i) The density of partons in the central region is likely to become rather large during the nuclear collision: First, partons from different nucleons overlap spatially, and second, there is an enhanced production of additional, new partons through multiple emission processes. Therefore the reverse processes of parton absorption become important. The net emission rate will decrease until emissions and absorptions locally reach a detailed balance.

(ii) The radiation emitted by a virtual parton has a specific formation time which results in the Landau-Pomeranchuk effect [18]. If the density of partons becomes large, so that there is a good chance that a parton undergoes multiple scatterings in a short time interval, then the radiation this parton wants to emit is suppressed.

(iii) An important feature of parton radiation is the interference of soft gluons. It reduces the multiplicity of produced partons due to destructive interference [20,30–32]. This effect, which is claimed to be significant already in e^+e^- annihilation and in pp and $p\bar{p}$ collisions [31], is of particular importance if the number of low-energy gluons becomes large. This is expected in heavy-ion collisions as the system thermalizes.

1. Competitive emission and absorption

To take into account absorptive processes according to the parton densities in phase space the naive emission rate of partons in multiple branchings is modified to an effective rate. Suppose that in some order N of perturbation theory we have evaluated the amplitude A_N for an outgoing parton a of momentum p_a [Fig. 2(a)]. It is convenient to visualize the correction associated with the branching $a \to bc$ as the "decay" of parton a into b and c. For example, the lowest-order Born amplitude A_0 represents the decay $e \to cd$ of a virtual parton e into outgoing partons c and d [Fig. 2(b)]. In the absence of any other partons, the first-order correction A_1 results exclusively from an emission of one additional parton from either one of the two outgoing partons. In Fig. 2(c) this contribution is labeled $A_1^{(+)}$ and is illustrated as $e \to a+d$ with the subsequent emission of a parton b, $a \to b + c$. However, in the presence of a significant number of neighboring partons in the relevant region of phase space, for each of the branching processes $q \to qg$, $g \to gg$, $g \to q\bar{q}$ there will be a competing absorption process, namely, $qg \to q$, $gg \to g$, $gq \to q$ with amplitude $A_1^{(-)}$. In Fig. 2(d) it is depicted as $e \to a+d$ followed by the absorption of a parton b, $a+b \to c$. In the frame where $p_e \equiv q = (Q, \mathbf{0})$, the corresponding lowest-order rate dR_0, the emission rate $dR_1^{(+)}$, and the absorption rate $dR_1^{(-)}$ are

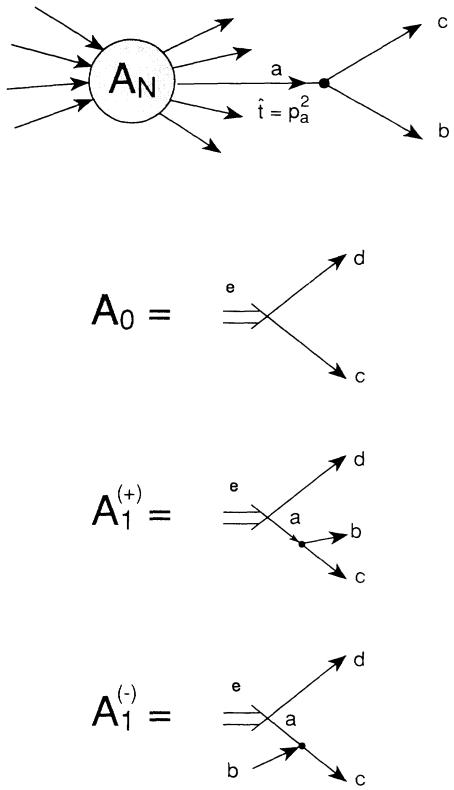

FIG. 2. Top part: Graphical representation of the Nth-order amplitude A_N^a for the production of a parton a with momentum p_a and invariant mass $\hat{t} = p_a^2$, and the next-order correction associated with the branching $a \to bc$. Lower part: Diagrams for the lowest-order Born amplitude A_0 and the first-order corrections $A_1^{(+)}$ and $A_1^{(-)}$ for the emission and absorption of an additional parton, respectively.

$$dR_0 = \frac{1}{2Q}\frac{d^3p_c}{(2\pi)^3 2E_c}\frac{d^3p_b}{(2\pi)^3 2E_d}[1 \pm F_c(p_c)][1 \pm F_d(p_d)]\sum |M_{e\to c+d}|^2 (2\pi)^4\delta^4(q - p_c - p_d) \ , \tag{42}$$

$$dR_1^{(+)} = \frac{1}{2Q}\frac{d^3p_b}{(2\pi)^3 2E_b}\frac{d^3p_c}{(2\pi)^3 2E_c}\frac{d^3p_b}{(2\pi)^3 2E_d}[1 \pm F_b(p_b)][1 \pm F_c(p_c)]$$
$$\times[1 \pm F_d(p_d)]\sum |M_{e\to b+c+d}|^2 (2\pi)^4\delta^4(q - p_b - p_c - p_d) \ , \tag{43}$$

$$dR_1^{(-)} = \frac{1}{2Q}\frac{d^3p_b}{(2\pi)^3 2E_b}\frac{d^3p_c}{(2\pi)^3 2E_c}\frac{d^3p_b}{(2\pi)^3 2E_d}F_b(p_b)\,[1 \pm F_c(p_c)] \times[1 \pm F_d(p_d)]\sum |M_{e+b\to c+d}|^2\,(2\pi)^4\delta^4(q+p_b-p_c-p_d)\ . \tag{44}$$

As before, the distribution functions $F_\alpha(p_\alpha) \equiv F_\alpha(p_\alpha, \mathbf{r}, t)$ are the phase-space densities of partons of type α with four-momenta p_α at given $\mathbf{r}$ and time t, and $\sum |M|^2$ are the squared matrix elements, summed over spin and color and weighted by a factor $[1 \pm F_\alpha(p_\alpha)]$ for each outgoing parton, with $-$ for $\alpha = q, \bar{q}$ and $+$ for $\alpha = g$.

By making use of the symmetry relation $\sum |M_{e\to b+c+d}|^2 = \sum |M_{e+b\to c+d}|^2$ the emission rate (43) and absorption rate (44) can be combined to an effective net rate:

$$dR_1 = dR_1^{(+)} - dR_1^{(-)} = \left(1 - \frac{F_b(p_b)}{1 \pm F_b(p_b)}\right) dR_1^{(+)}\ . \tag{45}$$

The relative contribution of emission and absorption processes to the total rate $dR_0 + dR_1$ is obtained by factorizing out the lowest-order rate dR_0 to yield the relative probability

$$d\mathcal{P}_{abc} = \frac{dR_1}{dR_0}\ . \tag{46}$$

Introducing the variables $z = E_b/E_a$ and $\hat{t} = p_a^2$ one finds, in the "leading pole approximation [33],"

$$d\mathcal{P}_{abc} = \left(1 - \frac{F_b(z,\hat{t})}{1 \pm F_b(z,\hat{t})}\right)\frac{\alpha_s(\hat{t})}{2\pi\hat{t}}\,P_{a\to bc}(z)dz\,d\hat{t} \tag{47}$$

with the usual Altarelli-Parisi functions [34]

$$\begin{aligned} P_{q\to qg}(z) &= \frac{4}{3}\left(\frac{1+z^2}{1-z}\right), \\ P_{g\to gg}(z) &= 6\,\frac{[1-z(1-z)]^2}{z(1-z)}, \\ P_{g\to q\bar{q}}(z) &= \frac{1}{2}\,[z^2 + (1-z)^2], \end{aligned} \tag{48}$$

and $\alpha_s(\hat{t})$ is given by Eq. (40). The expression (47) recovers the ordinary relative emission probability of the leading pole approximation if the phase-space density $F_b(z,\hat{t})$ is zero. However, if $F_b(z,\hat{t})$ grows during the nuclear collision, emission processes will be increasingly suppressed until a balance between emissions and absorptions is reached. Furthermore, Eqs. (47) and (48) exhibit the usual collinear $(d\hat{t}/\hat{t})$ and infrared (dz/z) singularities, which when integrated over produce the leading logarithmic divergence. However, in a dense parton system the increased absorption probability due to a large phase-space occupancy $F_b(z,\hat{t})$ may act as a natural cutoff for collinear and soft emissions, a point that remains to be investigated.

2. *The Landau-Pomeranchuk effect*

The Landau-Pomeranchuk effect [18,35,36] is a consequence of the specific space-time evolution of radiation emitted by an accelerated charge and can be observed in the bremsstrahlung of electrons. When a charge undergoes multiple scatterings in a medium and the time between the successive scatterings is shorter than the "formation time" of the radiation, then the contribution from intermediate scatterings cancel out, resulting in an effective suppression of radiation. This effect is expected to occur also for the radiative gluon emissions of partons in relativistic heavy-ion collisions [35,36], where partons may encounter multiple scatterings shortly after each other.

A simple way to incorporate this effect into the framework of multiple parton emissions of Sec. II E 1 is to estimate the formation time of radiation from a timelike virtual parton through its lifetime τ, as given by the formulas (39). The probability that a parton a with timelike virtuality $\hat{t} = p_a^2$ decays within a time interval Δt is given by $\Pi_a(\sqrt{\hat{t}}, \Delta t)$ according to Eq. (41). Thus, multiplying the relative emission probability $d\mathcal{P}_{abc}$ (47) with the decay probability Π_a yields

$$d\tilde{\mathcal{P}}_{abc} = \Pi_a(\sqrt{\hat{t}}, \Delta t)\left(1 - \frac{F_b(z,\hat{t})}{1 \pm F_b(z,\hat{t})}\right)\frac{\alpha_s(\hat{t})}{2\pi\hat{t}}\,P_{a\to bc}(z)dz\,d\hat{t}\ . \tag{49}$$

This expression gives the probability that the branching $a \to bc$ occurs within the time interval Δt. Since the time scale of the process is $\tau_a \propto E_a/\hat{t} = E_a/[z(1-z)k_\perp^2]$ where $k_\perp$ is the transverse momentum spread of b and c, large angle emissions preferably happen within rather short times, whereas more soft and collinear emissions are delayed. Note however that in Eq. (49) the introduction of a time delay for an emission through the function

Π_a is based on the classical picture of treating a timelike virtual parton a as an excited state that decays after a lifetime corresponding to its off shellness [cf. Eq. (41)]. This finite lifetime prevents an instantaneous, irreversible emission and mimics the possibility that the parton rescatters before it radiates. On the other hand, the Landau-Pomeranchuk effect is actually caused by the phenomenon that a parton "shakes off" its color field in the first scattering, and, until this field is regenerated, subsequent scatterings of the "half dressed" parton may occur, without intermediate radiation [35]. It is obvious that these are two different physical pictures. Nevertheless, Eq. (49) effectively takes into account the formation time of the radiation and is therefore a first approximation to incorporate the Landau-Pomeranchuk effect in a simple manner in the model. It can, in principle, be refined along the formalism presented in Refs. [35,36].

3. *Effective form factors for multiple parton emission and absorption*

Integrating Eq. (49) over the kinematically allowed region of the energy variable z gives the effective probability that during a change $d\hat{t}$ a parton a may branch into b and c within a time interval Δt. In the "leading logarithmic approximation" [20] the probability for a cascade of multiple, connected branchings becomes a product of probabilities for each single branching. Summing up the cumulative effect of many small changes $d\hat{t}$ one obtains the probability for *no* branching to occur. When written as a form factor, it provides a convenient basis for Monte Carlo simulation of multiple branchings [30–32]. For a timelike cascade, initiated by a parton a with virtuality $p_a^2 = M_a^2$, proceeding as a tree of successive branchings of partons with decreasing virtualities $M_i^2 > M_{i+1}^2$, the form factor T_a is obtained on the basis of Eq. (46):

$$T_a(M^2,\mu_0^2) = \exp\left\{-\int_{\mu_0^2}^{M^2}\frac{dM'^2}{M'^2}\Pi_a(M',\Delta t)\sum_b\int_{z_{\min}(M'^2)}^{z_{\max}(M'^2)}dz\left(1-\frac{F_b(z,M'^2)}{1\pm F_b(z,M'^2)}\right)\frac{\alpha_s(\tilde{M}'^2)}{2\pi}P_{a\to bc}(z)\right\}. \quad (50)$$

This form factor gives the probability that a parton a does *not* branch between M^2, the invariant mass associated with the vertex at which it was produced, and a minimal invariant mass $\mu_0^2 < M^2$ in a specified time interval Δt. The argument in α_s is generally a function of M^2 and z; here it is chosen as $\tilde{M}^2 = z(1-z)M^2 \simeq k_\perp^2$ [30–32].

In the case of a spacelike cascade of parton branchings, one asks for the probability that a primary parton b which encounters its first collision at some scale Q_b^2 might have evolved from a previous spacelike branching $a \to bc$ at $|q'|^2 < Q_b^2$, while the parton a itself may be a product of a preceding branching at $|q''|^2 < |q'|^2$, and so forth. This "backward evolution" [37–39] of the spacelike cascade reconstructs the parton virtualities from the q_b^2 value implied by the scattering of the primary parton b back to the initial resolution scale Q_0^2 of the incoming nuclei and takes into account the Q^2 evolution of the initial nuclear structure functions. The corresponding form factor S_b gives the probability that parton b has not originated from a preceding branching $a \to bc$ between Q_b^2 and $Q_0^2 < Q_b^2$ [38]:

$$S_b(x_b,Q^2,Q_0^2) = \exp\left\{-\int_{Q_0^2}^{Q^2}\frac{dQ'^2}{Q'^2}\frac{\alpha_s(Q'^2)}{2\pi}\sum_a\int_{\tilde{z}_{\min}(Q'^2)}^{\tilde{z}_{\max}(Q'^2)}d\tilde{z}\left(\frac{x_a f_a(x_a,Q'^2)}{x_b f_b(x_b,Q'^2)}\right)P_{a\to bc}(\tilde{z})\right\}. \quad (51)$$

Here $x_\alpha = (p_\alpha)_z/P$ $(\alpha = a,b)$ are the longitudinal momentum fractions of the partons' parent nucleons, $\tilde{z} = x_b/x_a$ is the fractional momentum of parton b taken away from a, $f_\alpha(x_\alpha,Q^2)$ are the corresponding nucleon structure functions, as in Eq. (3), and $Q^2 = Q_b^2$ is associated with the scale of the scattering vertex of parton b.

4. *Soft gluon interference*

The form factors (50) and (51) correspond to the summation of dressed ladder diagrams without interference, in a physical gauge, and sum up the leading collinear logarithmic contributions to all orders in α_s. However, when soft gluons are present there are additional contributions that are less singular in collinear directions, but have compensating infrared singularities. In the leading logarithmic approximation some of these collinear logarithms are then replaced by infrared ones. In contrast with the leading collinear singularities these new terms cannot be associated with dressed ladder diagrams in a physical gauge. They necessarily involve interference between soft gluon radiation from different partons. Nevertheless, the interference can be taken into account in a modified form of the parton branching processes using the soft gluon techniques originally developed by Basetto, Ciafaloni, and Marchesini [20].

The modifications required for a proper inclusion of

leading infrared singular contributions are rather simple [30]: parton emission is still described by successive branchings but the available phase-space is reduced to an angular ordered region in which the branching angles are ordered in a decreasing sequence. Outside the angular ordered region the coherence of different emission diagrams leads to destructive interference. The angular variable

$$\xi = \frac{p_b \cdot p_c}{E_b E_c} \simeq 1 - \cos\theta_{bc} \tag{52}$$

replaces the parton virtuality M_a^2 as evolution variable in the form factor (50) for timelike cascades. The two variables are related by

$$M_a^2 = M_b^2 + M_c^2 + 2E_bE_c\xi \simeq 2E_bE_c\xi = 2z(1-z)E_a^2\xi \tag{53}$$

where $z = E_b/E_a$ and $(1-z) = E_c/E_a$, as in Eq. (47). Furthermore, the argument of α_s in (50) is replaced as $\tilde{M}^2 = z(1-z)M^2 \to 2z^2(1-z)^2E_a^2\xi$.

As long as the parton energies are all of the same order of magnitude, angular ordering is equivalent to ordering the parton virtualities and the result of the two procedures will be similar [30–32]. But when some parton energies are much smaller than others the ordering of angles is a stronger constraint, corresponding to the suppression of disordered configurations.

For spacelike cascades the different kinematics are expected to prevent soft gluon interference to play as important a role as in the timelike processes, because the ordering of virtualities in this case imposes a natural angular ordering that inhibits interference [30]. Therefore, the evolution variable in the spacelike form factor (51) is taken to be the parton virtuality Q^2.

F. Comments on assumptions and approximations of the model

After having outlined the framework of the parton cascade model and introduced the newly included features, I believe it is very important to point out clearly the limitations and shortcomings of the approach. Since the model is a combination of a variety of physical mechanisms, it is conducive to disentangle the theoretically rather well understood components from the more phenomenological elements. In addition there are a number of assumptions and open questions on which I would like to comment with the following critical remarks (see also Ref. [2]).

(1) The parton cascade model is a semiclassical approach to model some of the numerous complex mechanisms that predominantly govern the dynamics of high energy nuclear collisions. It is based on a classical transport equation for the single-particle distributions of partons, in which the collision term is constructed on the basis of renormalization-group-improved QCD perturbation theory. The central assumption is here that (at least during the early stage of the nuclear reactions) the dynamics is essentially driven by binary parton-parton collisions in which the partons are treated as classical, pointlike particles that interact through independent scatterings with associated radiative emissions and absorptive processes. This means, although these perturbative QCD processes are firmly established by experimental evidence, their interplay, as incorporated in the model, is a purely Abelian approximation. Furthermore, the presence of a long-range color field and color correlations among the partons are neglected. There are numerous theoretical works in the literature attempting a rigorous derivation of a closed kinetic theory of quarks and gluons, based on quantum mechanical Wigner functions and the Dirac and Yang-Mills equations [40]. It has been shown that, in addition to the appearance of a number of specifically non-Abelian terms in the collision integrals, a self-consistent regularization of the arising infrared singularities requires the use of generalized Lenard-Balescu terms [41]. These issues and many other, to date, poorly understood aspects of a correct quantum theoretical kinetic formulation are beyond the scope of this paper. It should be clear that the model presented here is a much more "nuts and bolts" approach that avoids the tremendous complexity of these problems, but that benefits from the intuitively underlying picture and the opportunity to actually perform practical calculations.

(2) Aside from formal theoretical objectives it needs to be emphasized that the model combines the rather well understood dynamics of parton cascades [20] in the framework of perturbative QCD with a number of relatively bold phenomenological elements. In particular, the most crucial assertions and approximations concern (i) the ansatz for the initial parton distribution of the colliding nuclei, (ii) the extrapolation of (semi)hard parton collisions to a phenomenological soft scattering region, (iii) the use of free-space matrix elements together with a medium independent cutoff for the parton momentum transfer in scatterings and the invariant mass cutoff for emitted gluons, which stand in for a dynamical regularization, ultimately provided by thermal parton propagators and color screening in dense quark-gluon matter, and (vi) the scheme to model the Landau-Pomeranchuk effect that estimates the formation time for radiative emissions in a rather simplified way by treating the virtual partons as unstable excitations with a finite lifetime.

(3) There are several phenomena that may be of importance for the dynamical evolution of the system of partons in high-energy nuclear collisions, but which are (up to now) completely neglected in the current model. The most important, I believe, are the following.

(i) Parton shadowing: There is clear experimental evidence [42] for "nuclear shadowing," an effect that is evident in a depletion of the quark structure functions in a nucleus relative to a free nucleon at small momentum fractions $x \leq 0.1$. Considerable theoretical effort within various models [43] has been made to understand this effect. Relatively recently also "gluon shadowing," the expected similar behavior of the gluon structure functions, has been addressed [44,45]. Although there is no clear experimental signal for this yet, gluon shadowing is especially of interest for high-energy nuclear collisions, because it may significantly influence the initial condi-

tions in such a reaction. In particular, it has been shown in Ref. [45] that the single-particle inclusive $p_\perp$ spectra in proton-nucleus and nucleus-nucleus collisions should exhibit a clear observable supression due to gluon shadowing. These quark and gluon shadowing effects are not included in the present parton cascade model, but can in principle effectively be implemented in a similar fashion as in, e.g., Refs. [45,46].

(ii) Fluctuations and particle correlations: Aspects of "color transparency," concerning fluctuations in the spatial extension of the partons inside the nucleons of the initial nuclei, are neglected. Color transparency, which has been studied in the context of hadron-nucleus collisions [47], is the expected property of QCD that the possibility of small-size, almost pointlike parton configurations in a nucleon results in a smaller interaction probability with the target. It has been claimed however, that at RHIC energies this effect practically should disappear [48]. Nevertheless, correlations between, e.g., the partons' flavors and positions or momenta may be of interest, because the form of the initial phase-space distribution of partons clearly affects the dynamical conditions of the nuclear collision. However, because of the current lack of a more detailed experimental knowledge of correlations among flavor, momentum and spatial distribution of the partons in the nucleons, the ansatz of Sec. II B should be a sufficient approximation. Furthermore, in accord with the form of the transport equation (1), the parton distributions are to be interpreted as single-particle distributions which average over the correlations in the many-body system. Effects of two-particle correlations on the parton level have recently been studied in simulations of minijet production in hadron-hadron collisions [49]. The theoretical understanding of such correlations is still very incomplete. For experimental observables in the mean they should be irrelevant.

(4) Finally, some remarks on Lorentz invariance and gauge invariance. It is well known that a Lorentz-invariant many-body theory must necessarily be of many-time nature, even at the classical level: each particle carries its own proper time. On the other hand, the structure of any conventional cascade calculation is that the (three-dimensional) variation of spatial distance for every possible pair of particles is followed to arrange the ordering of binary collisions taking place in cascades (i.e., which pair collides first, which next, etc.). Since the spatial distance separation is not a Lorentz invariant quantity, the time ordering of collisions can be different from one reference frame to another. The distance of closest approach $(r_{ab})_{\min}$ between two particles a and b that must be compared with the interaction radius $\sqrt{\hat{\sigma}_{ab}/\pi}$ to determine whether a collision occurs is most clearly understood in the c.m. frame of the pair. The transformation of the distance of separation r_{ab} to a Lorentz frame moving with velocity β relative to the c.m. frame of a and b is $r_{ab}^2 \to r_{ab}'^2 = r_{ab}^2 + \gamma^2(\boldsymbol{\beta}\cdot\mathbf{r}_{ab})^2$. Now, the most relativistic parton-parton scatterings are those between energetic partons emerging directly from the two incoming nuclei. The vector minimum distance $\mathbf{r}_{ab}$ for such pairs is almost perpendicular to the beam direction. This property will be true in any Lorentz frame moving in the beam direction. Therefore the minimum distance of approach $(r_{ab})_{\min}$ is almost Lorentz invariant under such a Lorentz transformation. I have checked this property numerically by comparing collisions in the total nuclear c.m. frame and the target rest frame, with negligible differences in the results when transformed from one frame to the other.

Concerning the radiative emission and absorption processes of partons, the question of Lorentz invariance is inevitably connected with the choice of the kinematic variables used in the description. For timelike processes, the choice of $\xi = p_a\cdot p_b/E_aE_b$ and $z = E_b/E_a$ (Sec. II E 4) guarantees approximate Lorentz invariance [31]. A violation of Lorentz invariance arises in principle from the noninvariance of the energy fraction z, but it has been shown in Ref. [31] that this effect is negligible. Similarly, for spacelike branchings the choice of the invariant parton virtuality $-q^2$ and the momentum fraction $\tilde{z} = x_b/x_a$ (Sec. II E 3) provides an almost Lorentz invariant description of the branching process, except for small violations of rotational invariance associated with z.

Turning to the problem of gauge invariance, the parton cascade approach meets a fundamental problem: the parton-parton scattering amplitudes with off-mass shell partons in the initial or final state of the vertex are not gauge invariant. This is of relevance when timelike virtual partons-partons propagate and rescatter before they have returned on mass shell. However, the majority of timelike partons have relatively small virtualities, close to the mass shell, because most of the parton-parton scatterings, which provide them with this virtual excitation, involve a moderate momentum transfer. Only in the rare truly hard scatterings partons get scattered far off-mass shell. Therefore the violation of gauge invariance should be small in the mean. Nevertheless, a satisfactory implementation of gauge invariance in the parton cascade approach remains a conceptual problem which needs to be addressed in the future.

III. CENTRAL COLLISIONS OF S+S AND Au+Au AT RHIC

The results presented are devoted to central ^{32}S+^{32}S and ^{197}Au+^{197}Au collisions, respectively, at RHIC with c.m. energy $\sqrt{s} = 200A$ GeV (A=32, 197). The method of solving the transport equation (1) for time evolution of the parton distributions during the nuclear collisions by Monte Carlo simulation is described in Ref. [2]. At certain points in time the phase-space distributions, number and types of interactions, etc., were extracted to provide the information for the analysis below. The results shown were obtained by averaging over 25 runs for S+S and 5 runs for Au+Au. In the mean there were about 1300 (7500) particles initially and 2200 (17 800) at the end of the evolution for S+S (Au+Au). Statistical uncertainties are very small, typically of the order of one percent or less for the number of partons and for the particle spectra at their maximum.

Four fundamental parameters are involved in the calculations. First, the QCD scale parameter Λ that con-

trols the coupling strength α_s, Eq. (40), and determines the scale dependence of the nuclear structure functions in spacelike parton branchings, is chosen in accord with the structure function parametrization of Ref. [12]:

$$\Lambda = 0.2 \text{ GeV} . \tag{54}$$

Next, the resolution scale Q_0 for the initial parton structure of the colliding nuclei and the invariant-mass cutoff μ_0 for the virtualities of final-state partons, which define the regime inbetween which the parton distributions are evolved perturbatively. The value of Q_0 is evaluated dynamically during the calculation [as explained in Sec. II B after Eq. (7)],

$$Q_0 = \begin{cases} 1.9 \text{ GeV} & \text{for S+S,} \\ 1.7 \text{ GeV} & \text{for Au+Au,} \end{cases} \tag{55}$$

whereas μ_0 is taken to be fixed:

$$\mu_0 = 1 \text{ GeV} . \tag{56}$$

Finally, the scale $Q_{\text{cut}} = p_{\perp\text{cut}}$ that separates hard and semihard parton collisions from soft interactions is chosen according to Eq. (30):

$$p_{\perp\text{cut}} = 1.54 \text{ GeV}/c . \tag{57}$$

A. Parton multiplicities and characteristics of the space-time evolution

Figures 3–5 show some characteristic features of the dynamics of parton interactions and the space-time evolution of the system. To study the effects of the space-time structure of parton interactions, discussed in Sec. II, two extreme *evolution scenarios* were considered.

(a) Parton scatterings occur instantaneously without time delay. Associated cascades of successive parton branchings evolve immediately at the same space-time

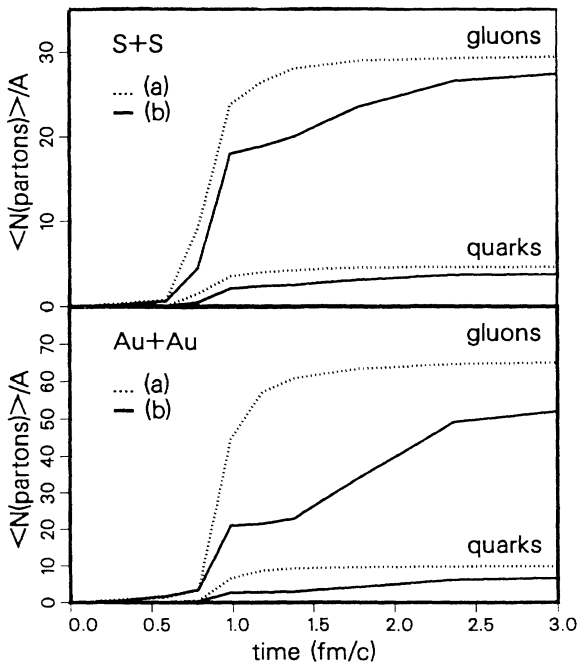

FIG. 3. Average cumulative number of secondary gluons and quarks per nucleon produced during collisions of ^{32}S+^{32}S and ^{197}Au+^{197}Au at $\sqrt{s} = 200A$ GeV. The plots (a) and (b) refer to the two space-time evolution scenarios explained in the text.

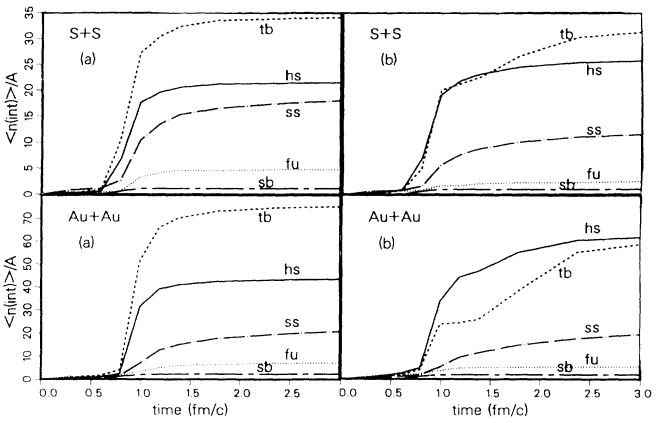

FIG. 4. Time evolution of the average cumulative number of the various parton interactions in ^{32}S+^{32}S and ^{197}Au+^{197}Au collisions at $\sqrt{s} = 200A$ GeV: hard and semihard scatterings (hs), soft scatterings (ss), time-like branchings (tb), space-like branchings (sb), and parton fusions (fu). The figure labels (a) and (b) correspond to the two evolution patterns discussed in the text.

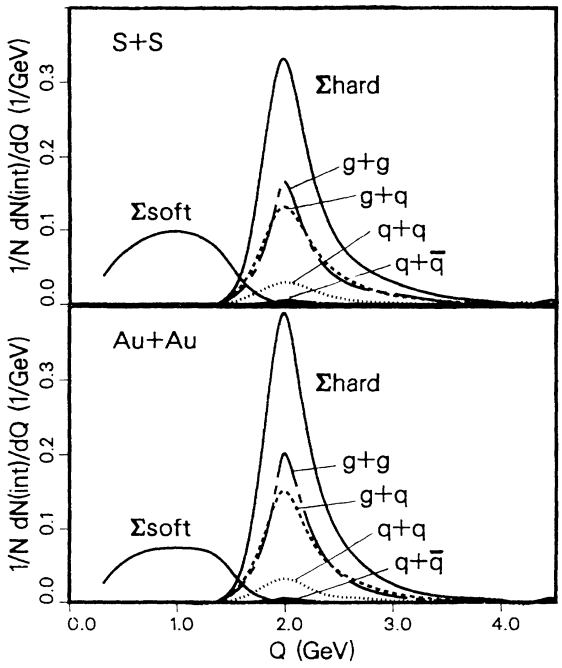

FIG. 5. Relative contributions of (semi)hard and soft parton-parton collisions in ^{32}S+^{32}S and ^{197}Au+^{197}Au ($\sqrt{s} = 200A$ GeV). Shown are the differential probabilities dP_{int}/dQ as a function of $Q = p_\perp$ (full lines). The (semi)hard collisions are in addition split up into the individual contributions from $g+g$, $g+q$, $q+q$, and $q+\bar{q}$.

point as the scattering vertex (zero formation time for radiative emissions). Absorptive processes and soft gluon interference are switched off. This evolution pattern corresponds to the one of Ref. [2].

(b) The time scale of each individual parton collision is taken into account and the subsequent parton branchings are delayed according to the characteristic formation time for the emissions. Absorptions of partons compete with the emissive processes and soft gluon interference decreases the available phase space for low energetic gluon bremsstrahlung.

In Fig. 3 the average cumulative number of secondary partons per nucleon is displayed as a function of time in the total c.m. frame for S+S [Fig. 3(a)] and Au+Au [Fig. 3(b)]. The dotted and full lines correspond to the evolution scenarios (a) and (b), respectively. Here and in the following the term *secondary partons* refers to all those partons that have evolved from initial spacelike virtual states to real states (on mass shell or timelike) as well as newly created partons, resulting from spacelike or timelike branchings. Accordingly, *primary partons* are initial-state partons that have not encountered any collision. In comparing the curves in Fig. 3 for scenarios (a) and (b) it becomes evident that in the latter case the multiplicity of secondary partons is significantly lower and the evolution of the system is dilated. Also, these effects are more prominent for Au+Au [about 20 percent lower multiplicity in case (b)] than for S+S [about 10 percent lower multiplicity in case (b)]. Furthermore, an obvious feature of scenario (b) is the sudden temporary suppression of parton production following the explosive increase at $t \simeq 0.6$ fm/c. The reason for this behavior is the abrupt production of a large number of partons within a very short time which gives rise to a dense phase-space population. The particle emission from excited partons is effectively suppressed because many partons encounter multiple scatterings and cannot emit radiation immediately. In addition the absorption of partons by others becomes important as the system responds to the high density. It turns out that for Au+Au the significant reduction of the number of produced partons can be attributed roughly as follows: 40 percent from the Landau-Pomeranchuk effect, 35 percent from absorption of partons, and 25 percent from the effect of coherent parton branchings with soft gluon interference.

Figure 4 shows the contributions of the various interaction processes as the system evolves in time. The average cumulative numbers of $2 \rightarrow 2$ collisions (hard and soft scatterings), of $2 \rightarrow 1$ branchings (timelike and spacelike branchings), and of $2 \rightarrow 1$ fusion processes are depicted for S+S and Au+Au. Figures 4(a) and 4(b) refer to the evolution scenario (a) and (b), respectively. One sees that the relative contributions from soft scatterings (ss) are less important compared to hard scatterings (hs) in both scenarios, but especially in scenario (b). This supports the dominance of perturbative QCD processes. The contributions from timelike branchings (tb) resemble the curves in Figs. 3 for the number of produced partons and again reflect the effects of suppression of radiative emissions in scenario (b). Spacelike branchings (sb) play a neglectable role in all cases. This is because the virtualities of the initial partons are chosen according to the average momentum transfer of primary parton collisions, as outlined in Sec. II B. As a consequence, spacelike branchings arise only from a few hard primary collisions with momentum transfers considerably larger than the partons initial virtuality. Finally, the parton-fusion processes (fu) are less prominent in scenario (b) for two reasons. First, the multiplicity of soft partons (which are the prime candidates for fusions) at early times is generally lower in case (b) since it takes longer for these partons to "evaporate" their relatively small excitation. Second, the parton absorption processes included in the form factor of timelike branchings partly take over the role of decreasing the number of partons.

In summary, Figs. 3 and 4 exhibit that the spacetime evolution according to scenario (a) is characterized by a very short time scale, in which a large number of partons is produced almost instantaneously, whereas scenario (b) exhibits a dilated evolution with a significantly smaller multiplicity of produced partons. In the following only the more realistic evolution pattern (b) is considered.

In Fig. 5 the relative probabilities $P_{\rm int}(Q) = (1/N_{\rm int})dN_{\rm int}(Q)/dQ$ for soft and hard parton-parton collisions are shown as functions of the interaction scale $Q = p_\perp$. Below $p_{\perp\rm cut} = 1.54$ GeV/c the partons interact via soft collisions. The interaction probability tends to zero at vanishing $p_\perp$ because most of the soft collisions still provide an appreciable momentum transfer. Above $p_{\perp\rm cut}$ the hard collisions govern the dynamics. However, most of these scatterings are not "hard" at all; rather, their distribution in $p_\perp$ is peaked at 2 GeV/c with a steeply falling tail $\sim p_\perp^{-5}$. Genuinely hard collisions are rare. Also shown in Figs. 5 is the separation of the hard scatterings into the contributions from the various collision channels. The most important contributions come from $g + g$ and $g + q$ scatterings which shows the dominant role of gluons for the dynamical evolution. Note that gluon radiation from excited gluons and quarks in addition enhances the number of gluons in the system.

B. Density evolution

The time evolution of the number densities of partons is shown in the first two columns of Figs. 6 and 7 for S+S and Au+Au at $\sqrt{s} = 200A$ GeV, respectively. The spatial region occupied by the partons has been divided into cells and the number of (primary and secondary) partons have been counted in each of them at different stages of the collision. The first column gives the density profile in the longitudinal (z) direction along the collision axis, whereas the second column shows the profile in the transverse ($r_\perp$) direction. The nuclear center of mass coincides with $z = r_\perp = 0$. Plotted are the normalized distributions $\rho(z) = (1/N)dN/dz$ and $\rho(r_\perp) = (1/N)dN/d^2r_\perp$. The full curves represent all (primary and secondary) partons present, whereas the dotted lines show the fraction of primary partons.

At time $t = 0$ fm/c the nuclei are about to touch each other. The shape of the incident longitudinal profiles clearly exhibit the thin slabs of valence quarks that are

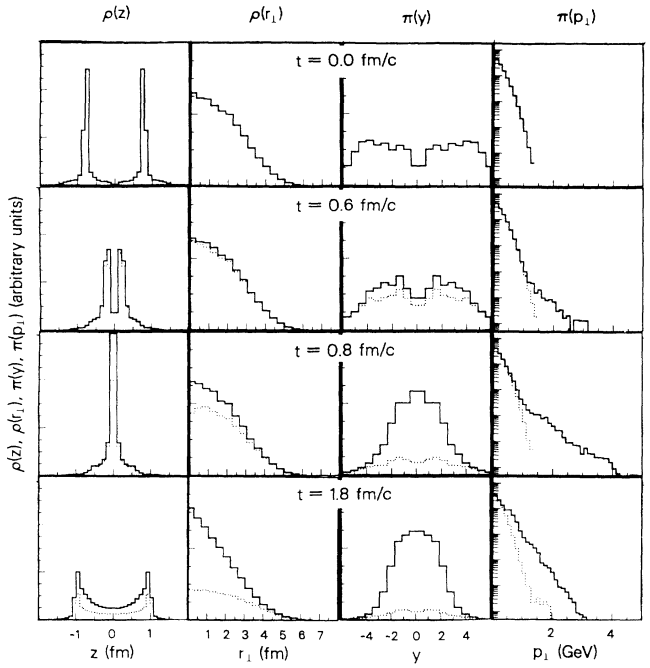

FIG. 6. Time evolution of the spatial distributions $\rho(z) = (1/N)dN/dz$, $\rho(r_\perp) = (1/N)dN/d^2r_\perp$ and the rapidity and transverse momentum spectra $\pi(y) = (1/N)dN/dy$, $\pi(p_\perp) = (1/N)dN/d^2p_\perp$ in $^{32}S+^{32}S$ collisions at $\sqrt{s} = 200A$ GeV. The full histograms refer to the sum of primary and secondary partons, whereas the dotted lines indicate the contribution of primary partons only. Note, $\pi(p_\perp)$ refers to partons with $|y| \leq 2.5$ and is plotted in a logarithmic scale.

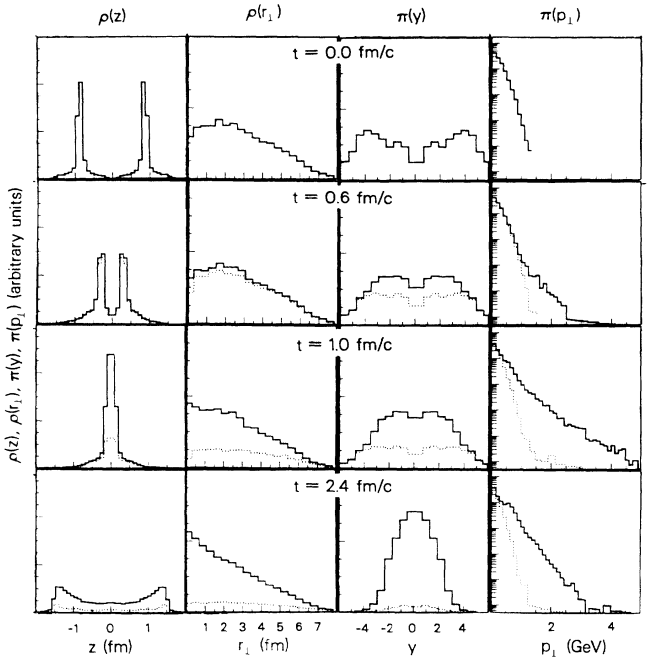

FIG. 7. The density profiles $\rho(z) = (1/N)dN/dz$, $\rho(r_\perp) = (1/N)dN/d^2r_\perp$ and the momentum distributions $\pi(y) = (1/N)dN/dy$, $\pi(p_\perp) = (1/N)dN/d^2p_\perp$ at various times during $^{197}Au+^{197}Au$ collisions at $\sqrt{s} = 200A$ GeV. Full histograms represent the sum of primaries and secondaries whereas dotted lines show the contribution of exclusively primary partons. The $p_\perp$ distribution refers to partons with $|y| \leq 2.5$. Note the logarithmic scale.

surrounded by clouds of gluons and sea quarks. The initial transverse distribution reflects the Fermi shape of the nuclei. Notice the following features: (i) Although the nuclei begin to overlap at $t = 0$ fm/c, it takes about 0.8–1 fm/c until they are on top of each other. (ii) Along the beam direction the matter is progressively compressed and reaches a maximum compression at $t \simeq 0.8$–1 fm/c. (iii) A dense population of secondary partons is built up inbetween the fast receding beam fronts as the system decompresses in the longitudinal direction. (iv) There is no indication of an appreciable squeeze-out up to $t =$ 1.8 (2.4) fm/c in the $r_\perp$ distributions in Fig. 6 (7). The system expands almost exclusively along the beam axis and exhibits cylindrical symmetry.

Shortly after the moment of maximum compression, most of the secondary partons produced in the central region are excited and, on average, almost at rest. The system is quite "hot" and the partons seem to represent the property of a (combined) single lump of matter.

C. Momentum distributions

The third and fourth columns of Figs. 6 and 7 show the time evolution of the rapidity (y) distributions $\pi(y) = (1/N)dN/dy$ and the transverse ($p_\perp$) distributions $\pi(p_\perp) = (1/N)dN/d^2p_\perp$ for S+S and Au+Au at $\sqrt{s} = 200A$ GeV. The distributions are obtained in the total c.m. frame at a certain time t by integration over all $\mathbf{r}$ and over $\mathbf{p}_\perp$, respectively, y. In contrast with the density profiles in the first two columns, the momentum spectra include only valence quarks and secondary partons, since only these contribute to the reaction dynamics. The full lines show the total distributions whereas the dotted lines exhibit the contribution of primary partons only. Initially all partons are primary, therefore the full and dotted curves coincide in the plots for $t = 0$ fm/c and correspond to the initial valence quark distribution.

It is evident that the region of small rapidity is quickly populated, reflecting the production of excited partons in the central rapidity region with a considerable fraction of the partons' kinetic energy being converted into timelike virtual masses. At the compressed stage (t =0.8–1 fm/c) the system can be viewed as a collection of a large number of excited secondary partons nearly at rest crossed by the remnants of the two opposite initial flows. At the end of the evolution the initial bumps around $|y| = 4$ have been almost completely depopulated and a narrow central plateau has been developed around $y = 0$ with a width of about 1–2 rapidity units [50].

For the $p_\perp$ distributions a cut on the partons with $|y| \leq$

2.5 has been imposed to focus on the central rapidity region. The initial Gauss distribution with $\langle p_\perp \rangle = 0.38$ GeV/c rapidly develops a tail for $p_\perp \geq 1$ GeV/c which decreases continuously until the distribution approaches an exponential shape and an average final $\langle p_\perp \rangle \simeq 0.65$ GeV/c.

D. Quark-gluon plasma formation

I turn now to the question of equilibration of the parton system (the formation of a quark-gluon plasma in the central collision region) and the thermalization time τ_{eq}. The characteristic time scale for quark-gluon plasma formation (usually termed "formation time" τ_0) has been given different meanings in the literature and estimates, ranging over more than an order of magnitude, have been made within rather different models. For example, Bjorken [51] interpreted it as an initial time for imposition of boundary conditions of hydrodynamic flow and assumed it $\simeq 1$ fm/c. Hwa and Kajantie [6] give $\simeq 0.1-0.2$ fm/c for the time scale after which thermalization in a small central phase-space cell is complete. Blaizot and Mueller [9] understood it as the time at which the partons are "freed" through their very first collisions with others, estimating $\simeq 0.2 - 0.3$ fm/c. Finally, Shuryak [10] gets a global equilibration time of $\simeq 2$ fm/c in a two-stage equilibration scenario. In comparing the numbers, one has to distinguish whether they refer to "local" thermalization within a microscopic space-time cell, or to "global" thermalization with respect to a comparably macroscopic volume composed of many such small cells. Of course local thermalization in individual cells is the first step for the system to equilibrate globally and the respective time scales can easily differ by an order of magnitude.

In the following I will address only the approach to global equilibration in the central region, defined to be a cylindrical volume of $\simeq 34$ fm^3 for S+S, or 180 fm^3 for Au+Au. I will refer to the time during which the system reaches equilibrium in the central region as τ_{eq}. I define the equilibration time τ_{eq} to be the time span between (i) the ignition of parton collisions at proper time τ_i and (ii) the time τ_f when the parton momentum distributions do not exhibit any further longitudinal slowing down, and the quanta in the central region have essentially harnessed the initial kinetic energy for their interactions. These points of time are determined as follows.

(i) To specify the actual beginning of the reaction on the parton level, t_i, measured in the nuclear c.m. frame, I plot in Fig. 8 the spatial distribution of vertices where secondary partons are produced versus time in the nuclear c.m. frame. Shown are the distributions in longitudinal (z) and transverse ($r_\perp$) direction for S+S and Au+Au. One sees that it takes a time

$$t_i \simeq 0.6 \text{ fm}/c \tag{58}$$

after the moment the nuclei began to overlap ($t = 0$ fm/c) until parton interactions substantially pick up (also evident from Figs. 3 and 4). This point of time corresponds

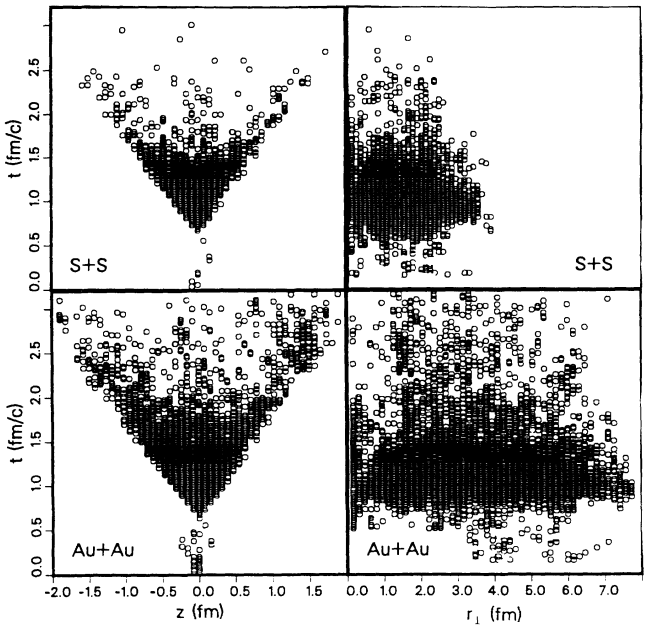

FIG. 8. Distribution of vertices of the production of secondary partons in longitudinal (z) and transverse ($r_\perp$) direction during central collisions of ^{32}S+^{32}S and ^{197}Au+^{197}Au. The point $t = 0$ fm/c is the moment the nuclei begin to overlap.

to the second rows of Figs. 6 and 7. It is obvious from the longitudinal density profiles that the very few collisions occurring before t_i are those between the partons in the clouds of gluons and sea quarks that precede the highly contracted slabs of valence quarks.

(ii) The reaction is essentially complete when the momentum distributions of partons become stable and do not exhibit any further change as the particles move apart. From analyzing the evolution of the rapidity and transverse momentum spectra, it turns out that a stabilization is achieved after

$$t_f \simeq 1.8 \ (2.4) \ \text{fm}/c \tag{59}$$

for S+S (Au+Au). Although, as is obvious from Figs. 3(b) and 4(b), the interactions among partons and especially branching processes continue up to 3 fm/c, they do not contribute significantly to the reaction dynamics. There is no appreciable further time variation of the distributions observable up to 3 fm/c, when the calculations have been stopped. Furthermore, from Fig. 9, which shows the time evolution of transverse energy per nucleon produced by secondary partons, $E_\perp/A = (1/A)\sum_i \sqrt{p_i^2 + m_i^2}$, in various bins Δz along the beam axis and centered at the c.m., it appears that for S+S (Au+Au) at $t_f \simeq 1.8$ (2.4) fm/c the curves coincide for all slabs up to $|z| \leq 0.6$ (0.8) fm, implying a constant value of $E_\perp/A \simeq 7$ (10) GeV over a longitudinal range of 1.2 (1.6) fm.

From these considerations the conclusion is that the proper equilibration time τ_{eq} is approximately ($\tau = \sqrt{(t-t_i)^2 - z^2}$ for $t \geq t_i$)

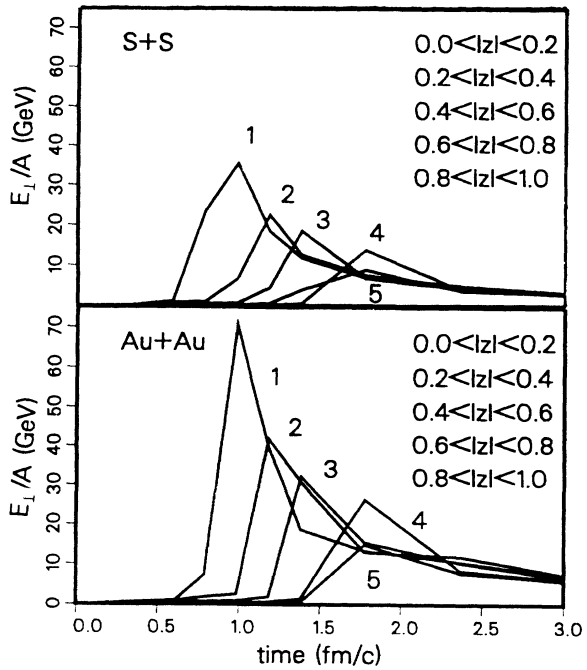

FIG. 9. Production of transverse energy per nucleon, $E_\perp/A$, by secondary partons versus time in bins along the collision (z) axis for ^{32}S+^{32}S and ^{197}Au+^{197}Au at $\sqrt{s} = 200A$ GeV.

$$\tau_{\rm eq} = \tau_f - \tau_i = t_f - t_i|_{z=0} = \begin{cases} 1.2\,{\rm fm}/c & \text{for S+S,} \\ 1.8\,{\rm fm}/c & \text{for Au+Au.} \end{cases} \tag{60}$$

Turning to the associated temperatures of the system in the central region, one observes from Fig. 6 (7) that at $t_f = 1.8$ (2.4) fm/c the final y and $p_\perp$ distributions exhibit a thermal shape. Note however that the transverse momentum distribution can easily show a close resemblance with a thermal distribution even though the total (or rapidity) distribution may still be distant from equilibrium. One has to be careful in drawing conclusions when relying on projected distributions to indicate the form of the full momentum distribution. To reveal the degree of thermalization in a more accurate way, one would have to analyze the full phase-space distribution in the six phase-space variables. This program is carried out in Ref. [3]. Here I will follow a more crude approach to estimate the approximate temperatures in the central region. In order to extract "effective" rapidity (longitudinal) and transverse temperatures, I tried to fit them with an appropriate thermal form. The fits are made with relativistic Boltzmann distributions which are good approximations to Fermi-Dirac and Bose-Einstein functions at high temperatures where quantum statistical effects can be neglected to a good approximation. Written in terms of y, $p_\perp$, the space-time rapidity $\eta = \frac{1}{2}\ln[(t+z)/(t-z)]$, and proper time $\tau = \sqrt{(t-t_i)^2 - z^2}$ the distributions are given by [6]

$$F(y, p_\perp, \eta, \tau = \tau_{\rm eq}) = F_0 \exp\left[-\frac{p_\perp}{T}\cosh(y-\eta)\right], \tag{61}$$

where the temperature $T \equiv T(\tau)$ serves as a fit parameter. The corresponding y and $p_\perp$ distributions are obtained by integrating over η and over $p_\perp$, respectively, y. The resulting fits are shown in Fig. 10. The sensitivity of the fits is such that the transverse temperatures $T_\perp$ are determined within an accuracy of 10 MeV whereas the uncertainty in the longitudinal temperatures T_y is about 20 MeV. The histograms are the final spectra from Figs. 6 and 7. Whereas the $p_\perp$ distribution is easily reproduced by adjusting the temperature T in Eq. (61) to the slope, the y distribution is too broad for a perfect thermal distribution, because it has a plateau shape of about two units of rapidity around $y = 0$. In order to describe the plateau, I superposed a theta function $h\theta(\Delta y - y)$ with $\Delta y = 0.5$ (S+S), 0.3 (Au+Au), and the parameter h adjusted to give the height of the plateau. The temperature was then fixed to fit the slope of the y distribution for $|y| \leq 2.5$, the rapidity interval that corresponds to the window set for the $p_\perp$ distributions. From Fig. 10 one sees that the so-obtained longitudinal and transverse temperatures $T_y \simeq T_\perp$ within the uncertainties, implying that the system indeed appears to attain a state of approximate equlibrium in the central collision region.

The essential conclusion from these results is that rather hot quark gluon plasmas can be formed in central S+S and Au+Au collisions at RHIC, with effective

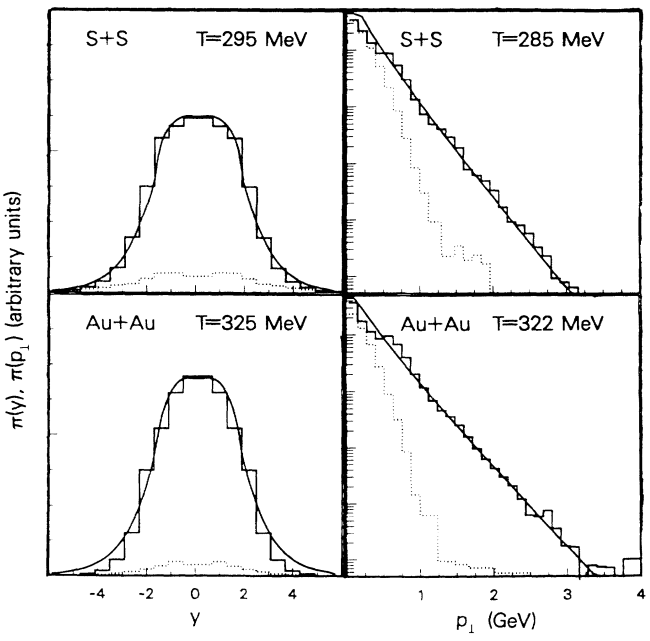

FIG. 10. Final rapidity and transverse momentum spectra of partons, $\pi(y) = (1/N)dN/dy$ and $\pi(p_\perp) = (1/N)dN/d^2p_\perp$ (the latter for $|y| \leq 2.5$) in central collisions of ^{32}S+^{32}S and ^{197}Au+^{197}Au at $\sqrt{s} = 200A$ GeV. The full (dotted) histograms correspond to all "real" partons (primary valence quarks only). The temperatures T are extracted by fits with relativistic Boltzmann distributions (full curves).

temperatures

$$T_0 \equiv T(\tau_{\rm eq}) \simeq \begin{cases} 290\,{\rm MeV} & \text{for S+S,} \\ 325\,{\rm MeV} & \text{for Au+Au,} \end{cases} \tag{62}$$

where the equilibration times $\tau_{\rm eq}$ are given in (58). Furthermore, in the central rapidity unit, the final momentum spectra give

$$\frac{dN}{dy} \simeq \begin{cases} 240 & \text{for S+S,} \\ 2600 & \text{for Au+Au,} \end{cases} \tag{63}$$

$$\frac{dE_\perp}{dy} \simeq \begin{cases} 160\,{\rm GeV} & \text{for S+S,} \\ 1700\,{\rm GeV} & \text{for Au+Au,} \end{cases} \tag{64}$$

with $\langle p_\perp \rangle = 0.67$ (0.64) GeV/c for S+S (Au+Au).

In order to estimate number densities and energy densities, I defined the central volume in S+S (Au+Au) to be a cylinder with length 1.2 (1.6) fm and radius 3 (6) fm centered at the center of mass. This region is nearly at rest with respect to the c.m. frame and the partons net velocity is small, as has been checked numerically. In this central region, the number densities and energy densities of secondary partons are calculated to give

$$n = \begin{cases} 12.6\,{\rm fm}^{-3} & \text{for S+S } (|z| \le 0.6 \text{ fm}, r_\perp \le 3 \text{ fm}), \\ 20.4\,{\rm fm}^{-3} & \text{for Au+Au } (|z| \le 0.8 \text{ fm}, r_\perp \le 6 \text{ fm}), \end{cases} \tag{65}$$

$$\varepsilon = \begin{cases} 17.1\,{\rm GeV/fm}^3 & \text{for S+S } (|z| \le 0.6 \text{ fm}, r_\perp \le 3 \text{ fm}), \\ 30.8\,{\rm GeV/fm}^3 & \text{for Au+Au } (|z| \le 0.8 \text{ fm}, r_\perp \le 6 \text{ fm}). \end{cases} \tag{66}$$

Clearly these numbers are to be understood as crude estimates for the densities, since it is averaged over the whole central volume. It seems that there is still a significant longitudinal flow at the edges of the considered volume, as is indicated by the relatively broad width of the y distributions in Fig. 10 and also by the large energy densities (66) as compared to the number densities (66). The energy associated with such a remaining longitudinal flow is contained in the estimates (66). Therefore the values given for the energy densities should be taken as upper estimates. For a more quantitative analysis of these points, I refer to Ref. [3].

It is instructive to compare the values for the energy densities (66) with the Boltzmann formula for a free gas of gluons and quarks:

$$\varepsilon = 3\,a\,T^4, \quad a = \frac{\pi^2}{90}\left(16 + \frac{21}{2}n_f\right). \tag{67}$$

The extracted temperatures (62) would give, taking into account $n_f = 3$ quark flavors, energy densities $\varepsilon = 14.3$ GeV/fm^3 for S+S and $\varepsilon = 22.5$ GeV/fm^3 for Au+Au. For $n_f = 4$ [52] one gets instead $\varepsilon = 17.4$ GeV/fm^3 for S+S and $\varepsilon = 27.5$ GeV/fm^3 for Au+Au. Although the formula (67) refers to an ideal gas of a noninteracting, massless partons, it is satisfactory to see that the model results are consistent within the uncertainties. Such notably high particle and energy densities would offer an appealing opportunity to study possibly new and interesting aspects of QCD in nuclear collsions, even independent of the question of quark-gluon plasma formation.

IV. CONCLUSIONS

From the study of ultrarelativistic nuclear collisions of ^{32}S+^{32}S and ^{197}Au+^{197}Au presented here within a kinetic parton cascade approach for the time development of the parton distributions, I conclude that in central collisions at RHIC hot quark gluon plasmas may well be established. The estimates for equilibration times, temperatures, and energy densities in S+S and Au+Au collisions predict $\tau_{\rm eq} = 1.2$ (1.8) fm/c, $T = 290$ (325) MeV, $\varepsilon = 17$ (31) GeV/fm^3. Effects of dilated emission from excited partons, the balance between radiative emissions and reverse absorption processes, and the interference of soft gluons have been shown to considerably affect the space-time evolution of the system, as compared to the case of Ref. [2] without these mechanisms. The most significant consequences are an extended duration of parton interactions resulting in longer equilibration times, and substantially lower multiplicities of produced secondary partons.

If this "hot parton" scenario of the early evolution of nuclear collisions is correct, then the proposed standard quark gluon plasma signatures should be clearly affected. The observable consequences should be [1,10] the following.

(i) *Enhanced production of charm.* Direct charm production in high-temperature quark-gluon plasmas is predicted to result in 0.7 $c\bar{c}$/event at RHIC [53,54], compared to "thermal" production yielding 0.01 (1) $c\bar{c}$/event at temperatures 300 (400) MeV. Therefore, the temperatures obtained in the present work would imply a significant increase of charm production as compared to pp collisions.

(ii) *Strangeness equilibration.* The enhancement of total strangeness [22,55] depends on the interrelation of the strange quark mass m_s and the thermal quark mass $m_{\rm th} \sim T$. For high temperatures as $T \simeq 300$ MeV and above the thermal mass is considerably larger and there should be no essential difference between initially produced u, d, and s quarks. If the multiple strange quark pairs, once produced, do not annihilate easily,

there should be an enhanced strangeness production observable.

(iii) *Direct Photon and lepton pair production.* The spectra of direct photons and dileptons produced during the early stage of the parton cascade evolution should exhibit a rather different behavior than the spectra obtained in the thermal scenario [56–58]. At early times most quark pairs are produced from "hot" gluons via $gg \rightarrow q\bar{q}$ and $g^* \rightarrow q\bar{q}$ and therefore should reflect the momentum distribution of the gluons with their high temperature.

ACKNOWLEDGMENTS

I am grateful for the helpful and encouraging discussions with J. Kapusta, L. D. McLerran, and B. Müller. The extensive numeric calculations were performed on Cray computers at the Minnesota Supercomputer Institute and the North Carolina Supercomputing Center and on a Silicon Graphics computer at Duke University. This work was supported by the U.S. Department of Energy under Contract No. DOE/DE-FG02-87ER-40328.

[1] See, e.g., *Quark Gluon Plasma*, edited by R. C. Hwa (World Scientific, Singapore 1990); *Quark Matter '91*, Proceedings of the Ninth International Conference on Ultrarelativistic Nucleus-Nucleus Collisions, Gatlinburg, Tennessee, 1991 [Nucl. Phys. **A544**, 1c (1992)]; *Quark Gluon Plasma Signatures*, edited by T. C. Awes *et al.* Proceedings of the International Workshop, Strasbourg, France, 1991, edited by V. Bernard *et al.* (Editions Frontieres, Gif-Sur-Yvette, France, 1991).

[2] K. Geiger and B. Müller, Nucl. Phys. **B369**, 600 (1992).

[3] K. Geiger, following paper, Phys. Rev. D **46**, 4986 (1992).

[4] K. Geiger, Phys. Rev. D (to be published).

[5] D. H. Boal, Phys. Rev. D **33**, 2206 (1986).

[6] R. C. Hwa and K. Kajantie, Phys. Rev. Lett. **56**, 696 (1986).

[7] R. C. Hwa, Phys. Rev. D **32**, 637 (1985).

[8] R. C. Hwa, in *Quark Matter '83*, Proceedings of the Third International Conference on Ultrarelativistic Nucleus-Nucleus Collisions, Upton, New York, 1983, edited by T. W. Ludlamd and H. Wegner [Nucl. Phys. **A418**, 559c (1984)].

[9] J.-P. Blaizot and A. H. Mueller, Nucl. Phys. **B289**, 847 (1987).

[10] E. Shuryak, Phys. Rev. Lett. **68**, 3270 (1992).

[11] In quantum mechanics the propagation of off-shell particles is exponentially damped according to their virtuality. In the parton cascade model here, virtual partons are propagated as if they were on mass shell, but with the essential difference that their distance of travel is limited due their finite lifetime that is associated with their virtuality.

[12] M. Glück, E. Reya, and A. Vogt, Z. Phys. C **48**, 471 (1990).

[13] V. M. Belyaev and B. L. Ioffe, Nucl. Phys. **B313**, 647 (1989).

[14] D. Antreasyan *et al.*, Phys. Rev. Lett. **48**, 302 (1983).

[15] T. D. Gottschalk, CERN Report No. TH.3810-CERN, 1984 (unpublished).

[16] J. D. Bjorken, in *Current Induced Reactions*, Proceedings of the International Summer Institute on Theoretical Particle Physics, Hamburg, 1975, edited by J. Körner *et al.*, Lecture Notes in Physics, Vol. 56 (Springer, New York, 1976).

[17] A. H. Mueller, in *Quark Matter '88*, Proceedings of the Seventh International Conference on Ultrarelativistic Nucleus-Nucleus Collisions, Lenox, Massachusetts, 1988, edited by G. Baym, P. Braun-Munzinger, and S. Nagamiya [Nucl. Phys. **A498**, 41c (1989)].

[18] L. D. Landau and I. Ya. Pomeranchuk, Dokl. Akad. Nauk SSSR **92**, 535 (1953); **92**, 735 (1953).

[19] L. V. Gribov, E. M. Levin, and M. G. Ryskin, Phys. Rep. **100**, 1 (1983).

[20] A. Bassetto, M. Ciafaloni, and G. Marchesini, Phys. Rep. **100**, 203 (1983).

[21] S. de Groot, W. A. van Leuwen, and C. G. van Weert, *Relativistic Kinetic Theory* (North-Holland, Amsterdam, 1980).

[22] T. Matsui, B. Svetitsky, and L. D. McLerran, Phys. Rev. D **34**, 783 (1986); **35**, 2047 (1986).

[23] H. Akama, J. Phys. Soc. Jpn. **28**, 478 (1970).

[24] H. van Erkelens, C. R. Acad. Sci. Paris **290B**, 293 (1980).

[25] N. Abou-El-Naga, K. Geiger, and B. Müller, J. Phys. G **18**, 797 (1992).

[26] E. Shuryak, Zh. Eksp. Teor. Fiz. **74**, 408 (1978) [Sov. Phys. JETP **47**, 212 (1978)].

[27] V. V. Klimov, Yad. Fiz. **33**, 1734 (1981) [Sov. J. Nucl. Phys. **33**, 934 (1981)]; H. E. Weldon, Phys. Rev. D **26**, 2789 (1982).

[28] R. Cutler and D. Sivers, Phys. Rev. D **17**, 196 (1978); B. L. Combridge, J. Kripfganz, and J. Ranft, Phys. Lett. **70B**, 234 (1977); B. L. Combridge, Nucl. Phys. **B151**, 429 (1979); E. Eichten, I. Hinchliffe, K. Lane, and C. Quigg, Rev. Mod. Phys. **56**, 579 (1984); **58**, 1065 (1986); P. Nason, S. Dawson, and R. K. Ellis, Nucl. Phys. **B303**, 607 (1988); **B327**, 49 (1989); **B335**, 260 (1990).

[29] G. Gustafson, Z. Phys. C **15**, 155 (1982); H. U. Bengtsson, Comput. Phys. Commun. **31**, 323 (1984).

[30] B. R. Webber, Annu. Rev. Nucl. Part. Sci. **36**, 253 (1986).

[31] G. Marchesini and B. R. Webber, Nucl. Phys. **B238**, 1 (1984); **B238**, 492 (1984);

[32] M. Bengtsson and T. Sjöstrand, Nucl. Phys. **B289**, 810 (1987).

[33] K. Konishi, A. Ukawa, and G. Veneziano, Nucl. Phys. **B157**, 45 (1979); R. D. Field, *Applications of Perturbative QCD*, Frontiers in Physics, Vol. 77 (Addison-Wesley, Redwood City, CA, 1989).

[34] G. Altarelli, Phys. Rep. **81**, 1 (1982); G. Altarelli and G. Parisi, Nucl. Phys. **B126**, 298 (1977).

[35] N. N. Nikolaev, Usp. Fiz. Nauk **134**, 369 (1981) [Sov. Phys. Usp. **24**, 531 (1981)].

[36] F. Niedermeyer, Phys. Rev. D **34**, 3494 (1986).

[37] G. Marchesini and B. R. Webber, Nucl. Phys. **B310**, 461 (1988).

[38] M. Bengtsson, T. Sjöstrand, and M. van Zijl, Z. Phys. C **32**, 67 (1986).
[39] T. D. Gottschalk, Nucl. Phys. **B277**, 700 (1986).
[40] H.Th. Elze and U. Heinz, Phys. Rep. **183**, 81 (1989); in *Quark Gluon Plasma* [1], p. 177; S. Mrowczynski, Phys. Rev. D **39**, 1940 (1989); in *Quark Gluon Plasma* [1], p. 185.
[41] A. V. Selikov, Phys. Lett. B **268**, 263 (1991).
[42] J. Ashman *et al.*, Phys. Lett. B **202**, 603 (1988); M. Arneodo *et al.*, *ibid.* **211**, 493 (1988).
[43] L. L. Frankfurt and M. I. Strikman, Phys. Rep. **160**, 235 (1988).
[44] F. E. Close, J. Qiu, and R. G. Roberts, Phys. Rev. D **40**, 2820 (1989); A. H. Mueller, Nucl. Phys. **B335**, 115 (1990).
[45] X.-N. Wang and M. Gyulassy, Phys. Rev. Lett. **68**, 1480 (1992).
[46] X.-N. Wang and M. Gyulassy, Phys. Rev. D **44**, 3501 (1991).
[47] L. L. Frankfurt and M. I. Strikman, Prog. Part. Nucl. Phys. **27**, 135 (1991); H. Heiselberg, G. Baym, B. Blaettel, L. L. Frankfurt, and M. I. Strikman, Phys. Rev. Lett. **67**, 2946 (1991).
[48] L. L. Frankfurt and M. I. Strikman, Phys. Rev. Lett. **66**, 2289 (1991).
[49] X.-N. Wang and M. Gyulassy, Phys. Rev. D **45**, 844 (1992); X.-N. Wang, "Studying Minijets via the $p_\perp$ dependence of Two-particle Correlation in ϕ," Duke University, Report No. DUKE-TH-91-30, 1992 (unpublished).
[50] The rapidities of the colliding nuclei are $Y = \pm 5.36$ at $\sqrt{s} = 200A$ GeV and it is obvious that the majority of partons have rapidities $|y| < |Y|$ corresponding to small momentum fractions.
[51] J. D. Bjorken, Phys. Rev. D **27**, 140 (1983).
[52] Accounting for $n_f = 4$ rather than $n_f = 3$ effective quark flavor degrees of freedom is motivated by the relative proportions of quarks in the central region at time $\tau_{\rm eq}$ resulting from the calculations. For both systems S+S and Au+Au the calculations give an appreciable amount of charm, specifically, $u : d : s : c \approx 37 : 35 : 23 : 5$. Clearly, Eq. (67) serves here only as a consistency check for the model calculations and the charm-quark mass certainly cannot be neglected as is justified for u, d, and s. For a more realistic comparison the quark masses and the relative fractions of gluons and quarks should be taken into consideration.
[53] A. Shor, Phys. Lett. B **215**, 375 (1988); **233**, 231 (1989).
[54] B. Müller and X. N. Wang, Phys. Rev. Lett. **68**, 2437 (1992).
[55] P. Koch, B. Müller, and J. Rafelski, Phys. Rep. **142**, 167 (1986).
[56] R. C. Hwa and K. Kajantie, Phys. Rev. D **32**, 1109 (1985).
[57] J. Kapusta, P. Lichard, and D. Seibert, Phys. Rev. D **44**, 2774 (1991).
[58] J. Kapusta, L. D. McLerran, and D. K. Srivastava, Phys. Lett. B **283**, 145 (1992).

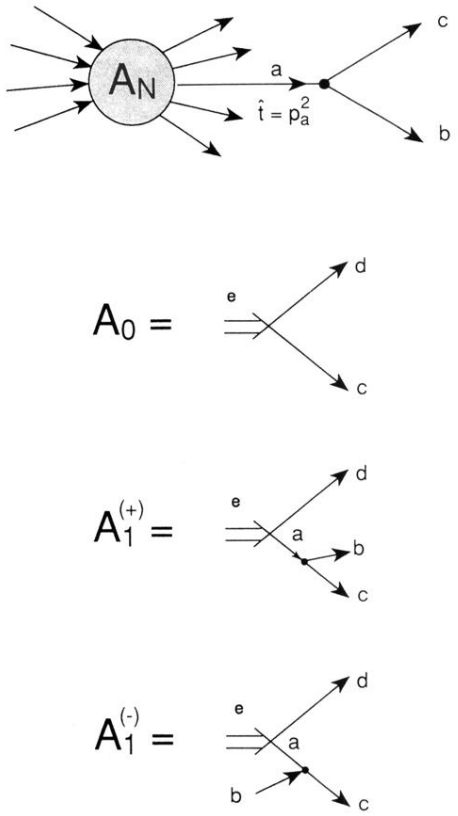

FIG. 2. Top part: Graphical representation of the Nth-order amplitude A_N^a for the production of a parton a with momentum p_a and invariant mass $\hat{t} = p_a^2$, and the next-order correction associated with the branching $a \to bc$. Lower part: Diagrams for the lowest-order Born amplitude A_0 and the first-order corrections $A_1^{(+)}$ and $A_1^{(-)}$ for the emission and absorption of an additional parton, respectively.

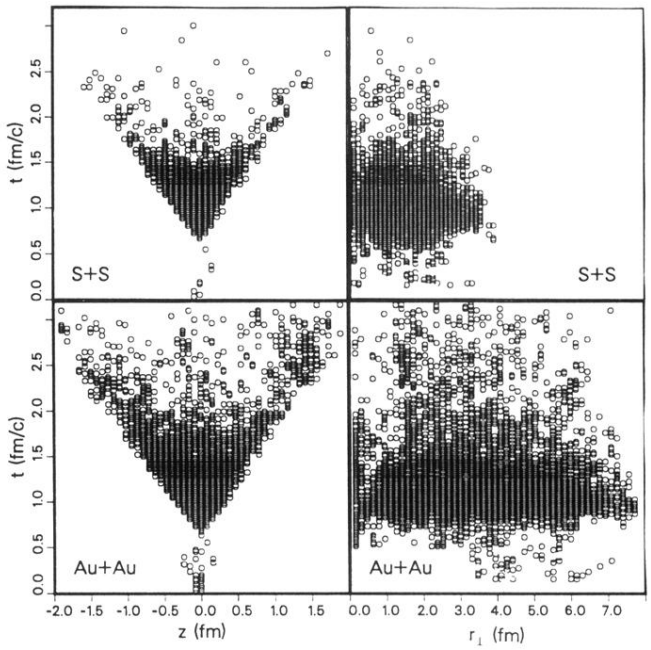

FIG. 8. Distribution of vertices of the production of secondary partons in longitudinal (z) and transverse ($r_\perp$) direction during central collisions of ^{32}S+^{32}S and ^{197}Au+^{197}Au. The point $t = 0$ fm/c is the moment the nuclei begin to overlap.